INTRODUCTORY SHEAR STRENGTH

Prepared by Dr. Roy E. Olson on Spring 1989

Modified by Jiunnren Lai on Spring 2004

INTRODUCTION

Failure in soils often means that one mass of soil begins sliding over another mass. The soil is said to fail in shear because the movement at the failure surface involves relative displacement parallel to the failure surface (Fig. 1). Several types of laboratory tests (direct shear, triaxial shear) were developed during the 1930's to measure the ability of soil to resist shearing stresses. These tests are still by far the most widely used and will be the main tests discussed in following chapters.

Although shearing tests can be performed in accord with standard specifications, the results may be misleading, and even dangerous, when applied in the analysis of an actual problem, unless the person who specifies the laboratory tests understands the factors that govern strength. Accordingly, this chapter deals with fundamental aspects of shearing strength of soils.

It is often convenient to refer to the shearing strength of a soil as if failure consisted of one rigid block of soil sliding over another. Actually, soils may undergo important movements prior to formation of a shearing surface and for loose soils, under drained conditions, no dominant shearing surface may form. Thus, it may be better to say that we are really interested in the overall stress-strain properties of soils with formation of a distinct shearing surface just representing an end product of a previous period of loading and straining.

FAILURE ENVELOPE IN DIRECT SHEAR

The simplest type of shear test, in principle, is direct shear (Fig. 2). Soil is confined inside a box, called the *shear box*, which provides complete confinement on the vertical sides, and then a normal force, N, is applied through the upper porous stone. The box is split on a horizontal surface. Half of the box (either the upper half or lower half) is held in place and the other half is forced to slide sideways. If the two halves of the box have either been separated slightly, or the contact surface between the boxes has been lubricated, then the applied shearing force is almost entirely resisted by shear in the soil. The ratio of the shearing force, F, to the area upon which shear is occurring in the soil, A, is the *shearing stress*, τ, and the ratio N/A is the *normal stress*, σ.

It is convenient to plot the results of direct shear tests in a *Coulomb diagram* with the shearing stress on the horizontal plane through the middle of the specimen plotted versus the normal stress. Such a plot for samples of a dry, dense, well graded, concrete sand is shown in Fig. 3. After the normal stress has been applied, and prior to application of any shearing stress, the stresses on the potential failure surface (horizontal surface) are located on the

horizontal axis in Fig. 3, e.g., at point A. As the horizontal force is gradually increased, the shearing stress, τ, increases and the stress state moves along the path AB in Fig. 3. The path AB is termed, a *stress path*. At point B the soil fails. If a series of direct shear tests are performed, using different values of the normal stress, then a number of stress paths can be plotted. It is found that the failure points lie along a line such as CD (Fig. 3). Samples with stresses that plot below the line CD are stable; samples with stress states on the line have failed; stress states above the line are not possible (subject to usual scatter in real data). The line CD is a *failure envelope* in that it envelopes all stable states of stress. The detailed shape, location, and orientation of the failure envelope depend on a number of factors which will be discussed subsequently.

For application in design, it is convenient to represent the failure envelope with an equation. The envelope is often slightly curved, especially if a wide range in normal stresses are used, but for the narrow ranges in u of interest on most projects, there is sufficient scatter in the actual data that the envelope can be approximated as a straight line (Fig. 3). The equation of the linear failure envelope is:

$$\tau = c + \sigma \tan\phi \qquad (16.1)$$

where c is the intercept (value of τ when σ is zero) and ϕ is the slope of the failure envelope. It is convenient to provide names for c and ϕ. Traditionally, c is termed the *cohesion* and ϕ the *angle of internal friction*. It is important to recognize from the beginning that, as defined here, cohesion is just the name of the intercept. It has no physical significance. Indeed, for the sand used in the tests shown in Fig. 3, the dry sand had no strength at a confining pressure of zero (it runs freely through your fingers) so the failure envelope must curve down to the origin at small normal stresses.

FAILURE ENVELOPES IN TRIAXIAL SHEAR

Introduction

Direct shear testing is useful for several classes of engineering problems but the device suffers from a number of important defects, as will be discussed in later chapters. A preferable test would be one in which the stresses and strains, and drainage conditions, in the sample are subject to better control. A device that provides much improved control of these factors is the triaxial shear device. The device was introduced in Chap. 15 and details will be presented in Chaps. 19 and 20; the concern here is with the measured shearing properties.

State of Stress

Triaxial shear tests are performed using solid cylindrical soil specimens. For the moment, it is only necessary to assume that the device makes it possible to subject the curved vertical surfaces of the specimen to a uniform normal stress (no shearing stress), and that the flat horizontal end surfaces can be subjected to a normal stress that may differ from the value for the curved sides. For current purposes, the horizontal stress will be called σ_h and the vertical stress σ_v (Fig. 4).

Planes (surfaces) subjected to no shearing stress are termed *principal planes* (or *principal surfaces*) and the normal stresses applied to these planes are termed *principal stresses*. It can be shown that any point in a stressed body there are three principal

planes and they are perpendicular to each other. The normal stresses on these principal planes may all have the same numerical value (*hydrostatic* state of stress) but more commonly the three principal stresses differ. It is convenient to give them special symbols, in particular σ_1 is the largest principal stress, σ_2 is the intermediate principal stress, and σ_3 is the smallest principal stress. Because stresses in the soil are usually compressive, it is convenient to define compressive stresses as positive and tensile stresses as negative.

In triaxial shear testing, σ_v (Fig. 4) is generally σ_1 and σ_h is σ_3, i.e., we push down on the specimen to cause it to fail. Such a test is called a triaxial compression test. On rare occasions, the lateral compressive stress is increased until failure occurs (σ_h becomes σ_1 and σ_v becomes σ_3); such a test is a triaxial extension test. It may be noted that only two principal stresses are subject to control and thus the test might better have been named a biaxial shear test.

Mohr Circle

In a triaxial test, failure must occur on sloping planes because no shearing stresses are assumed to occur in either vertical or horizontal planes. In order to plot a failure diagram, like the one shown in Fig. 3, we must be able to calculate the normal and shearing stresses on sloping planes.

Consider an element of soil with the surfaces subjected to σ_1 and σ_3 (Fig. 5) and assume that we want to calculate the stresses on a plane rotated through an angle a, counterclockwise from the plane upon which σ_1 acts (this is the positive direction for α). The plane AB (Fig. 5) is shown with positive stresses on it (σ is positive for compression and τ is positive if it tends to rotate the element OAB in the counterclockwise direction). If S is the length AB, then the lengths AO and BO are S cos(α) and S sin(α) respectively. For the element to be stable in the horizontal direction, the sum of the horizontal forces must be zero. If the element has a thickness (perpendicular to the page) of T, then the element is in equilibrium only if the horizontal stresses are in balance, i.e., if:

$$(\sigma_3)(T)(S)\sin(\alpha) + \tau \cos(\alpha)(T)(S) = \sigma \sin(\alpha)(T)(S) \qquad (16.2)$$

Similarly, equilibrium in the vertical direction requires that:

$$(\sigma_1)(T)(S) \cos(\alpha) = \sigma \cos(\alpha)(S)(T) + \tau \sin(\alpha)(S)(T) \qquad (16.3)$$

These equations can be solved simultaneously for iand a to obtain:

$$\tau = (\sigma_1-\sigma_3) \sin(\alpha) \cos(\alpha) \qquad (16.4)$$

$$\sigma = \sigma_1 \cos^2(\alpha) + \sigma_3 \sin^2(\alpha) \qquad (16.5)$$

With the help of the trigonometric identities that :

$$\sin (2\alpha) = 2 \sin(\alpha) \cos(\alpha) \qquad (16.6)$$

and:

$$\cos(2\alpha) = 1\text{-}2 \sin^2(\alpha) = 2 \cos^2(\alpha) - 1 \qquad (16.7)$$

Equations 16.4 and 16.5 can be converted to a more convenient form:

$$\tau = 1/2\ (\sigma_1-\sigma_3)\ \sin(2\alpha) \qquad (16.8)$$

$$\sigma = 1/2\ (\sigma_1+\sigma_3) + 1/2\ (\sigma_1-\sigma_3)\ \cos(2\alpha) \qquad (16.9)$$

Equations 16.8 and 16.9 are the *parametric* form of the equation of a circle (solution of Eqs. 16.8 and 16.9 using all possible values of the parameter α, and plotting the points, produces a circle) plotted in a τ-σ coordinate system (Fig. 6). Thus, each point on the circle represent a combination of τ and σ existing on a particular plane (a particular value of α). The circle, termed a *Mohr circle*, thus represents the state of stress (stresses on planes at any angle through the point) for planes perpendicular to the page, at a point in a stressed body. Mohr circles may be plotted for stresses in other directions to relate σ_1 and σ_2, or σ_2 and σ_3.

Note, in Fig. 6, that the central angle between the points representing the states of stress on planes acted upon by σ_1 and σ_3 is 180 degrees whereas the planes in space are only 90 degrees apart. The central angle in the Mohr's circle is always twice the angle between the associated two planes in space.

Suppose now that we perform a series of triaxial compression tests on samples of a soil. In each test the value of $\sigma_h = \sigma_2 = \sigma_3$ is held constant during the test and the test starts with no shearing stresses in the sample ($\sigma_1 = \sigma_2 = \sigma_3$). We shear the specimens by applying an additional axial stress, say σ_a, on top of the already existing stress, σ_3 to produce a total axial stress of σ_1. The numerical value of σ_a is clearly (σ_1-σ_3). Technically (σ_1-σ_3) is the "maximum principal stress difference" but we will shorten the name to just the *stress difference*. Some engineers have, unfortunately, termed the stress difference the deviator stress but that term was previously defined as the difference between any normal stress and the mean normal stress and thus should not be redefined in geotechnical engineering (Newmark, 1960; Schmid, 1960). A stress-strain curve for a triaxial test is shown in Fig. 7. This test was performed by applying a uniform rate of axial strain and measuring the resulting values of stress difference, thus allowing the test to be carried to strains in excess of the strain where the stress difference peaks (about 10 axial strain in Fig. 7). Failure may reasonably be defined to occur at the peak value of (σ_1-σ_3).

For each value of (σ_1-σ_3) we can plot a Mohr circle so the stress path curves of Fig. 3 for direct shear tests are now replaced by a series of circles (Fig. 8) for triaxial tests. For each test, the largest circle is the one at failure. Two lines (failure envelopes) can be drawn tangent to the largest circles. Smaller circles clearly represent stable states of stress. The tangent point between the envelope and the circles represents the state of stress on failure planes because the stresses on such planes plot on the failure envelope.

In plotting Mohr circles, it is clear that the part of the diagram below the horizontal line is the mirror image of the part above. Time and space are thus saved by plotting only the upper half.

From Figs. 6 and 8 we note that there are two values of 2α which correspond to failure planes. From Fig. 9 it is clear that 2α is + (90^o+ϕ) for one set of failure planes and - (90^o+ϕ) for the other set (the mirror image, not shown). Because angles in space are half of the associated central angles in the Mohr circles, the failure planes are located at angles of $\pm(45^o+\phi/2)$ from

the horizontal plane (plane upon rise which σ_1 acts) for compression tests and at the same angles measured from vertical planes for extension tests.

Modified Mohr-Coulomb Diagrams

Mohr-Coulomb diagrams are tedious to plot for a variety of reasons. Circles are difficult to draw, especially to obtain suitably dark lines for reproduction. When tests of several types are plotted, it is a problem to draw the circles in such a way as to show the different test types (dotted, dashed, ...). When many circles are plotted on the same diagram, the maze of lines obscures the results. It is also inconvenient to try to use statistical techniques to obtain the "best fit" failure envelope. These problems are easily resolved using modified Mohr-Coulomb diagrams. Consider the triangle OAB in Fig. 9:

$$\cos\phi = \frac{\frac{1}{2}(\sigma_1 - \sigma_3)}{\left[c + \frac{1}{2}(\sigma_1 + \sigma_3)\tan\phi\right]}$$

Thus, by rearrangement:

$$\frac{1}{2}(\sigma_1 - \sigma_3) = c \cdot \cos\phi + \frac{1}{2}(\sigma_1 + \sigma_3)\sin\phi \qquad (16.10)$$

If we plot $1/2(\sigma_1-\sigma_3)$ in place of τ and $1/2(\sigma_1+\sigma_3)$ in place of σ, (Fig.10), then each test is represented by a single point, greatly simplifying plotting. Different symbols can easily be used to represent differing conditions, e.g., in Fig. 10, boxes denote tests on normally consolidated specimens and triangles denote tests on specimens that were initially consolidated to a hydrostatic stress of 120 psi and then rebounded prior to testing (see later discussion of effects of drainage and over-consolidation). Regression analysis can easily be used to find the "best fit" failure envelope. Stress path curves are easily drawn. From Eq. 16.10, the slope of the envelope is $\sin(\phi)$, rather than $\tan(\phi)$ as in a regular Mohr-Coulomb diagram, and the intercept is c. $\cos(\phi)$ rather than c. The parameters c and ϕ are easily calculated. For example, suppose two points on the modified failure envelope are defined by :

(1) $\frac{1}{2}(\sigma_1 - \sigma_3)$ = 10.0 psi and $\frac{1}{2}(\sigma_1 + \sigma_3)$ = 20.0 psi

(2) $\frac{1}{2}(\sigma_1 - \sigma_3)$ = 20.0 psi and $\frac{1}{2}(\sigma_1 + \sigma_3)$ = 60.0 psi

Then:

$$\sin\phi = \frac{20-10}{60-20} = 0.25, \quad \phi = 14.5^o$$

c. $\cos\phi = 10.0 - (20)(0.25) = 5.0\ psi$

$$c = \frac{5}{\cos(14.5^o)} = 5.2\ psi$$

A second Modified Mohr-Coulomb diagram can be obtained by solving Eq. 16.9 for σ_1:

$$\sigma_1 = \left(\frac{2c\cos\phi}{1-\sin\phi}\right) + \sigma_3\left(\frac{1+\sin\phi}{1-\sin\phi}\right) \tag{16.11}$$

and plotting σ_1 in place of τ and σ_3 in place of σ. Again individual points are plotted and ϕ and *c* are calculated from Eq. 16.11. Finally, Eq. 16.11 can be converted to:

$$\sigma_1 - \sigma_3 = \left(\frac{2c\cos\phi}{1-\sin\phi}\right) + \sigma_3\left(\frac{2\sin\phi}{1-\sin\phi}\right) \tag{16.12}$$

and (σ_1-σ_3) plotted against σ_3. If the slope of the modified diagram is Ψ and the intercept *d*, then ϕ and *c* can be calculated using the equations shown in Table 16.1.

Table 16.1 Equations Used to Covert Parameters for Modified Mohr-Coulomb Diagrams to Standard Mohr-Coulomb Diagrams

Modified Ordinate	Abscissa	ϕ	*c*
$\frac{1}{2}(\sigma_1-\sigma_3)$	$\frac{1}{2}(\sigma_1+\sigma_3)$	$\text{Sin}^{-1}[\tan(\Psi)]$	$\frac{d}{\cos\phi}$
$\sigma_1-\sigma_3$	σ_3	$\sin^{-1}\left(\frac{\tan(\psi)}{2+\tan(\psi)}\right)$	$d\left(\frac{1-\sin\phi}{2\cos\phi}\right)$
σ_1	σ_3	$\sin^{-1}\left(\frac{\tan(\psi)-1}{\tan(\psi)+1}\right)$	$d\left(\frac{1-\sin\phi}{2\cos\phi}\right)$

Other Modified Mohr Coulomb diagrams have been developed as well. They all have the advantage of simplifying the plotting greatly while yielding exactly the same values of c and d) as for the more traditional, but cumbersome, Mohr-Coulomb diagram. The Modified Mohr-Coulomb diagram may be plotted using either total or effective stresses.

Effects of Drainage

Stages in laboratory tests In the triaxial apparatus the soil sample is sealed inside a membrane (see Chapter 19 for details) and it is a simple matter to provide one or more drainage lines so that water can be allowed to drain in or out of the specimen. In laboratory shear testing it is convenient to perform the test in two stages. The first stage occurs when the specimen is subjected to some initial state of stress and the second stage occurs when the stress state is changed in such a way as to cause failure (shearing stage). During the each stage the drainage lines can be open or closed. For preliminary considerations it is convenient to assume that stage one involves application of a hydrostatic state of stress(see later discussion).

Terminology During the application of the original hydrostatic stress, we state that the sample is either *unconsolidated* (valves closed, no flow in or out of the specimen) or *consolidated* (valves open, sample allowed to come to equilibrium with some predetermined value of pore water pressure). The terminology is unfortunate and tends to cause confusion because, although the "unconsolidated" sample is not consolidated in the laboratory during the triaxial test, the soil must have been consolidated previously to some finite value of

effective stress, in the laboratory or in the field, or it would have been too soft to handle. The terminology thus applies to the stage of laboratory testing, not properly to the condition of the specimen.

In any case, during the shearing stage, we also have two reasonable options; we close the valves, or we open the valves and shear the sample so slowly that the pore water pressures remain near some predetermined value. To avoid reuse of the word *consolidation*, we choose the word *drained* and say that the specimen is *undrained* or drained during shear.

The terms for the combined stages are then:

unconsolidated-undrained: the specimen is sealed throughout the test so the strength is measured at the same water content as in the sample had prior to being set up in the triaxial device.

consolidated-undrained: the sample is allowed to come to equilibrium under some state of stress, which presumably resembles a stress state in the field, and then is sheared undrained, to correspond to a field loading that occurs too rapidly to allow drainage.

consolidated-drained: the pore water pressure is maintained at some constant value throughout the test, presumably representing a field case where loads are applied so slowly that pore water pressures remain constant.

The unconsolidated-drained case is impossible because opening the valves for the second stage allows consolidation under the initial stresses to occur and a consolidated-drained test results. Names like unconsolidated-undrained are rather cumbersome. Shorthand notations of several types have been used:

unconsolidated-undrained:	UU,Q
consolidated-undrained:	CU, R
consolidated-drained:	D,CD,S

We will use the Q, R, S symbols most of the time because they are easily used as subscripts.

Pore water pressure coefficients Application of stresses to specimens results in the generation of pore water pressures (see Chapter 11). It is necessary to understand the pore water pressures in order to be able to understand the shearing properties of the soil. For the purposes of this introductory chapter, it will be assumed that the soil specimens are saturated. In considering pore water pressures, it is convenient to use dimensionless parameters, e.g., those suggested by Skempton (1954). The stresses applied to the exterior of a specimen can be separated into a hydrostatic component, say σ_h, and a shearing component, say $(\sigma_1-\sigma_3)$. If these stresses are changed by say $\triangle\sigma_h$ and $\triangle(\sigma_1-\sigma_3)$,then the change in pore water pressure, $\geq$u, is:

$$\triangle u = B\,[\triangle\sigma_h + A\triangle(\sigma_1-\sigma_3)] \qquad (16.13)$$

For saturated soils, B is somewhere between about 0.99 and 1.00 so B will be considered equal to one in this section. On the other hand, A varies with strain, with the state of stress during consolidation, with the stress state during shear, and with individual soil properties (see later discussions).

Q-compression tests A series of saturated samples of soil are placed in triaxial shear devices in the laboratory and are subjected to a range in hydrostatic stresses, σ_h. Prior to application of the hydrostatic cell pressure, each sample is exposed to the atmosphere and thus to a hydrostatic total stress (σ) of zero (gage pressure). The initial effective stress ($\bar{\sigma}$) in each sample is thus:

$$\bar{\sigma} = \sigma - u = -u$$

The initial pore water pressure in each sample is negative, thus causing each sample to have a positive effective stress. When each sample is subjected to a (different) confining pressure, σ_h:

$$\Delta\bar{\sigma} = \Delta\sigma - \Delta u = \sigma_h - B\sigma_h = 0$$

Thus, every sample has the same water content and effective stress at the beginning of the shearing stage. Further, shear induced pore water pressure and *compressive strengths*, $(\sigma_1\text{-}\sigma_3)_f$, are identical for all specimens in the series, even for specimens of sand (Bishop and Eldin, 1948). The failure envelope is thus horizontal when the normal stress axis is σ, the total stress.

In the special case that a compression test is performed with the minor principal total stress equal to zero (gage pressure), then the test is termed an *unconfined compression test*, and the compressive strength, $(\sigma_1\text{-}\sigma_3)_f$, is given the special symbol q_u. The unconfined compressive strength is the same as the compressive strength for a Q-type shear test with a finite confining pressure (Fig. 11) provided the degree of saturation remains constant. However, the degree of saturation usually drops below 100% during unconfined compression tests and the unconfined compressive strength is typically lower than the Q-type compressive strength (see later discussion of partially saturated soils).

We note, from Fig. 11 and the discussion above, that the compressive strength does not vary with the applied total stress. Thus, $\phi = \phi_Q = 0$ and $\tau_f = c_Q$ (note use of the test type as a subscript).

The term *compressive strength* was defined above as the stress difference at failure. It is convenient to define the *shearing strength* as the value of τ at failure. For a horizontal failure envelope:

$$\tau_f = c_Q = c_u = \frac{1}{2}(\sigma_1 - \sigma_3)_f \qquad (16.14)$$

where c_u is an often-used symbol for the undrained shearing strength.

S-compression tests For an S-type triaxial compression test, the specimen is usually first subjected to a hydrostatic stress and allowed to consolidate fully. Then the axial stress is increased at a rate slow enough to allow essentially full dissipation of the pore water pressures generated during shear. The shapes of the stress-strain curves vary depending on the overconsolidation ratio (see Chapter 11 for definition of overconsolidation ratio).

For normally consolidated soil, the increasing value of σ_1 causes the sample to decrease in volume during shear. For such a soil, the stress strain curves often have the shapes shown in

Fig. 12 (note that volumetric strain is defined as $\triangle V/V_0$, where V is total volume of the specimen, and V_0 is the volume at the beginning of shearing).

For highly overconsolidated samples, the volume typically decreases initially as σ_1 begins to increase, but then the sample begins to expand (Fig. 13). Often a shear plane forms when the sample begins to expand and failure occurs (peak stress difference).

The shearing stage during an S compression test involves a constant value of $\overline{\sigma}_3$ so the stress path is a line sloping at 45 degrees when is plotted $\frac{1}{2}(\sigma_1 - \sigma_3)$ against $\frac{1}{2}(\overline{\sigma}_1 + \overline{\sigma}_3)$, as shown in Fig. 10, or a verical line when $\frac{1}{2}(\sigma_1 - \sigma_3)$ is plotted against $\overline{\sigma}_3$, as shown in Fig. 14. The failure envelope typically has only a small cohesion intercept and_is often slightly concave downwards (Fig. 14). Clearly, the shearing strength, τ_f, depends on effective stress (Figs. 10 and 14) but not on total stress (Fig. 11).

Drained triaxial compression tests on normally consolidated and overconsolidated..samples of the same soil typically yield essentially identical failure enevelope, (Figs. 10 and 14), provided the soil is uncemented.

R-compression tests Two types of failure envelopes may be plotted from R-type compression tests. First, the R-envelope is defined using Mohr circles in which the minor principal stress of the Mohr circle is the effective stress at the beginning of the shearing stage, often denoted by the symbol $\overline{\sigma}_{3c}$ (denotes that this stress is the consolidation pressure) or $\overline{\sigma}_{3i}$ (denotes that σ_3 is the initial value of $\overline{\sigma}_3$ during the shearing stage). The diameter of the circle is (σ_1- σ_3), which has the same value in effective and total stresses, so:

$$\sigma_{1f} = \overline{\sigma}_{3c} + (\sigma_1 - \sigma_3)_f \qquad (16.15)$$

Although $\overline{\sigma}_{3c}$ and $(\sigma_1 - \sigma_3)_f$ are both effective stresses, σ_{1f} is not the major principal effective stress at failure because $\overline{\sigma}_{3c}$ is the minor principal effective stress at the beginning of shear, not at failure. As a result, some engineers refer to the R-envelope as a total-stress envelope. It is better to note that the confining pressure $\overline{\sigma}_{3c}$ is an effective stress and that the strength is increasing with this effective stress, and consider the R-envelope an effective-stress envelope.

It is possible to measure pore water pressures during the shearing stage so the effective stresses can be defined continuously. We will term such tests $\overline{R}$ tests to denote that current values of effective stresses are used. For normally consolidated samples, positive pore water pressures are generated during shear (Fig. 15). At the peak value of the stress difference the shear-generated pore water pressure is usually between about 0.5 and 1.5 times $(\sigma_1 - \sigma_3)_f$, i.e., the A coefficient (Eq. 16.13) typically ranges from as low as about 0.5 for some remolded samples to perhaps 1.5. For some soils, the pore water pressure continue to increase after "failure" whereas $(\sigma_1 - \sigma_3)$ typically decreases, leading to values of the A coefficient as much as five at large strain.

For highly overconsolidated samples, the dense arrangement of particles (compared with

normally consolidated specimens at the same stress state) usually leads to the sample tending to dilate (expand) during shear (Fig. 13) and this tendency leads to the development of negative pore water pressures (Fig. 16) when drainage is not allowed.

Stress-path curves for the two samples of kaolinite are shown in a Modified Mohr-Coulomb diagram in Fig. 17. The tendency of the highly overconsolidated sample to generate negative pore water pressures causes the stress path curve to move to the right, whereas the positive pore water pressures for the normally consolidated sample cause the stress path curve to move to the left.

Failure Criteria

Q, R, and S tests If we perform Q or S tests and plotstress path curve of (σ_1-σ_3) vs σ_3 (Q test) or $\overline{\sigma}_3$ (S test), the curves rise directly to the failure envelope (Figs. 11 and 14). Failure clearly occurs at the peak stress difference.

$\overline{R}$ tests In an R test on normally consolidated samples, a stress path curve can have the shape shown in Fig. 18. A failure envelope can be plotted through the points corresponding to the peak stress difference. However, the stress paths cross through this failure envelope into the region previously declared to be impossible to occupy. From Eq. 16.11 we can prove that:

$$\overline{\sigma}_1 = \overline{\sigma}_3 \tan^2(45+\frac{\overline{\phi}}{2}) + 2\overline{c}\tan(45+\frac{\overline{\phi}}{2}) \qquad (16.16)$$

(Note that (1+sinϕ)/(1-sinϕ) = $\tan^2(45+\phi/2)$. If there is no cohesion, then clearly $\overline{\phi}$ is a maximum when $\overline{\sigma}_1/\overline{\sigma}_3$ maximizes. This criterion is the *peak effective principal stress ratio* criterion. More generally, we can plot the stress paths and draw a failure envelope that is tangent to the curves, the failure criterion now being called the *stress path tangency* criterion (SPT for short).

Failure envelopes for a different kaolinite from that used previously, defined using the peak stress difference and the peak effective principal stress ratio are compared in Fig. 19. Values of $\overline{\phi}$ using the SPT and SD failure criteria are compared in Fig. 20. The view is widely held that. the difference between $\overline{\phi}$ values for the two failure criteria is a function of soil sensitivity (see Chap. 1 for definition of sensitivity). For convenience let:

$$R = \frac{\tan\overline{\phi}_{at(\sigma_1-\sigma_3)_{\max}}}{\tan\overline{\phi}_{at(\overline{\sigma}_1/\overline{\sigma}_3)_{\max}}} \qquad (16.17)$$

R can then be used as a measure of the effect of using the different failure criteria on the shearing strength (assuming negligible cohesion). Values of R from the published literature, for triaxial compression tests on undisturbed and essentially normally consolidated samples, are shown in Fig. 21. The scatter in Fig. 21 may result from lack of a relationship between R and sensitivity, but may also result from effects of additional variables, e.g., some of the tests may actually have been performed with overconsolidated soils, and testing errors may have influenced some of the results significantly.

Opinions as to which failure criterion should be used vary among knowledgeable people. It is clear, however, that for tests with normally consolidated specimens, the question is relevant only when the tests are strain controlled, i.e., when the samples are deformed at some selected rate and loads measured. In strain-controlled tests, deformation continues past the point of peak load. On the other hand, in a constant load test (where static loads are added to the specimen) application of the peak load typically leads to collapse of the specimen and the peak value of the effective stress ratio cannot be defined. Field problems in geotechnical engineering are load controlled. Consequently, the authors' opinion is that the peak stress difference criterion is the proper criterion if failure in the field is undarined.

ENERGY CORRECTIONS IN S TESTS

Direct Shear

In a direct shear test, the normal force is N and the shearing force is F. Consider what happens when the sample is at failure and is displaced horizontally by some small displacement, △h (Taylor, 1948, pp. 345-347). Suppose that the sample is expanding during this stage of the test and that it increases in thickness by △v. The work done on the sample is the force times displacement,

$$W_{in} = F \ \triangle h$$

The work done in the process involves a force used in shearing the sample, F^*, acting through △h Plus the work required to lift the normal force:

$$F \ \triangle h = F^* \ \triangle h + N \ \triangle v$$

Thus, the force shearing the sample, F^*, is:

$$F^* = F - N\frac{\Delta v}{\Delta h}$$

If there is negligible cohesion, then $\tan\bar{\phi}^*$ is F^*/N so:

$$\tan\bar{\phi}^* = \tan\bar{\phi} - \frac{\Delta v}{\Delta h}$$

If the sample is expanding during shear, then the corrected $\bar{\phi}$, $\bar{\phi}^*$, is less than $\bar{\phi}$ whereas $\bar{\phi}^*$ exceeds $\bar{\phi}$ when the sample is compressing at failure.

Triaxial Shear

Derivation of an equation such as Eq. 16.18 is much more difficult for triaxial tests. Bishop (1954) concluded that the stress difference in an S compression test should be corrected using:

$$(\sigma_1 - \sigma_3)^* = (\sigma_1 - \sigma_3) - \bar{\sigma}_3 \frac{d\nu}{d\varepsilon} \qquad (16.19)$$

where $(\sigma_1 - \sigma_3)^*$ and $(\sigma_1 - \sigma_3)$ are the corrected and uncorrected stress differences, respectively,

σ_3 is confining pressure, and $d\nu/d\varepsilon$ is the rate of increase in volumetric strain with respect to axial strain.

On the other hand, Bowe (1962) concluded that the correction should be of the form:

$$\sigma_1^* = \sigma_1 \frac{1}{(1 + d\nu / d\varepsilon)} \tag{16.20}$$

For most tests, the correction for the energy of volume change is small. Further, volume change occurs in the field also, so S type laboratory data should not be corrected for field application.

COMPARISON OF VALUES OF $\bar{\phi}$ BETWEEN DRAINED AND UNDRAINED TESTS

According to the principle of effective stress, the angle of internal friction of soils, expressed using effective stresses, should be the same whether the test is a drained or undrained test. Values of $\bar{\phi}$ are compared in Fig. 22 with $\bar{\phi}_R$ defined at the peak stress difference and with S data not corrected for the energy of volume change. In Fig. 23, values of $\bar{\phi}_R$ at the SPT point are compared with values of $\bar{\phi}_S$ corrected for the energy of volume change. Scatter in values may result from experimental errors (see later chapters). Generally, the principle of effective stress appears adequately validated.

EFFECTS OF OVERCONSOLIDATION ON SHEARING PROPERTIES

In many cases, soils in the field have been consolidated in the past to effective stresses exceeding the present values and a question arises as to the effect overconsolidation has on strength. The relationship of void ratio to consolidation pressure is shown in Fig. 24 for a clay that was remolded at a high water content and then consolidated under hydrostatic stress in the laboratory. The R and $\bar{R}$ failure envelopes, with failure defined at $(\sigma_1\text{-}\sigma_3)_{max}$ are shown in Fig. 25. The effect of overconsolidation on the $\bar{R}$ envelope is seen to be minor whereas a large hysteresis loop forms for the R envelope. When drained triaxial tests are used, the loop between the envelopes for normally consolidated and overconsolidated samples is small to nonexistent.

Some engineers find it convenient to express strengths from undrained shear tests using the c/p ratio. In the field, c/p is the ratio of the field undrained shearing strength to the effective vertical consolidation pressure. ln the laboratory, c/p is the secant slope (Ψ) in a modified Mohr-Coulomb diagram in whjch $1/2(\sigma_1\text{-}\sigma_3)$ is plotted versus $\bar{\sigma}_{1C}$ and a sample is initially consolidated under conditions of no lateral strain with $\bar{\sigma}_{1C}$ being the vertical consolidation stress. Representative data from Koutsoftas (1981) for tests on a marine clay are shown in Table _____. Clearly, c/p increases rapidly with degree of overconsolidation. Koutsoftas (1981) found that the ratio $(c/p)_{OC}/(c/p)_{NC} = OCR^m$ where subscripts NC and OC indicate normally consolidated and overconsolidated, OCR is the overconsolidation ratio, and m was found to range from 0.80 to 0.85. Ladd et al. (1977) found that m more generally ranged from 0.75 to 0.85. It should be noted that the main cause for the wide variation in c/p with respect to OCR is the effects of different pore water pressure. When effective

stresses at failure are used, the resulting failure envelopes are similar for normally consolidated and overconsolidated samples.

The relatively flat slope of the failure envelope for overconsolidated samples in the R tests may be used to estimate the maximum previous consolidation pressure (Chap. 11). The ratio of the undrained shearing strength to the effective consolidation pressure, often called simply the c/p ratio, is the slope of the R envelope for normally consolidated samples (see next section for effects of anisotropic consolidation pressures). If the slope of the rebound failure envelope is given by S, then the maximum previous consolidation pressure, say ρ_{max}. is given by:

$$\rho_{\max} = \frac{(c_f - SP_f)}{(c/p) - S} \tag{16.21}$$

where c_f and p_f are the measured strength and calculated effective overburden pressure in the field, respectively. The calculation is usually made after making the simplifying assumption that S is zero. This approach was tried by Anderson and Lucas (1981) for 46 cases and the values of ρ_{max} found using consolidation tests and strength tests was found to compare well provided the consolidation curve was not too rounded.

The Q envelope for saturated soils is horizontal so a horizontal envelope can be drawn through any point on the failure envelopes in Fig. 25 to define a Q envelope. If a comparison is made of the Q envelopes of normally consolidated and overconsolidated samples at a given consolidation pressure, $\overline{\sigma}_{3C} = \overline{\sigma}_{3i}$, overconsolidation clearly causes an increase in the undrained strength.

Overconsolidation causes the sample to be denser than a normally consolidated sample consolidated to the same stress state. While the normally consolidated sample tends to compress in a drained test, or generate positive pore water pressures in an undrained test, a highly overconsolidated (dense) sample tends to expand in a drained test or to generate negative pore water pressures in an undrained test. For example, values of the A coefficient (Eq. 16.10) at the peak stress difference are shown as a function of the overconsolidation ratio in Fig. 26. Stress path curves for normally consolidated and overconsolidated samples have different shapes because of the differing pore water pressures (Fig. 17).

EFFECTS OF ANISOTROPIC CONSOLIDATION ON UNDRAINED STRENGTH

In the laboratory it is convenient to consolidate samples, in the triaxial device, under a hydrostatic state of stress whereas in nature the soil is typically consolidated under conditions of essentially zero lateral strain. The ratio of the lateral effective stress to the vertical effective stress is the coefficient of earth pressure at rest, K_0. For normally consolidated soils, K_0 is typically about 0.5. For overconsolidated soils, K_0 is larger, with upper limits typically between two and three.

In Fig. 27, stress path AB is the one followed by a normally consolidated sample in undrained shear if it is originally consolidated to a hydrostatic stress at Point A, and then sheared to failure. Path ACD is for a specimen originally consolidated to the same hydrostatic stress, but then subjected to an increasing axial stress, σ_1, to point C under fully drained conditions, and then loaded to failure under undrained conditions along path CD. To simulate field conditions better, the anisotropically consolidated specimen could have been consolidated

along stress path OC first, and then sheared undrained along path CD. Clearly, for a normally consolidated soil, anisotropic consolidation Increases the ujidrained strength in comparison with another sample isotropically consolidated to the same lateral stress (strength at point D exceeds the strength at point B).

For overconsolidated samples, the effect of anisotropic consolidation may be to increase or decrease the undrained shearing strength depending on the degree of overconsolidation.

For a sample consolidated hydrostatically in the laboratory, the test begins with no applied shearing stress and the shearing stage must involve application of sufficient strain to raise the shearing stress from zero to the failure value. If the sample is consolidated anisotropically with $\overline{\sigma}_v = \overline{\sigma}_1$ and $\overline{\sigma}_h = \overline{\sigma}_c = \overline{\sigma}_3 = K_0\overline{\sigma}_1$, then a shearing stress exists at the start of the shearing stage (point C in Fig. 27). In a compression test, the shearing stress is simply increased until it reaches the failure value, thus only a small strain is required and the soil appears to be "brittle". On the other hand, if an extension test is performed, the shearing stress first is reduced to zero and is then increased to failure in the opposite direction so the required strain is large and the soil appears to be "plastic".

The A coefficient is also influenced by anisotropic consolidation. If the B coefficient is one, then the A coefficient is simply the ratio of the change in pore water pressure to the change in stress difference (Eq. 16.13). From the stress path curves in Fig. 27, it is clear that a significant pore water pressure will develop in the anisotropically consolidated specimen (path CD in Fig. 27) but that there will be only a small change in the stress difference. As an example, Henkel and Sowa (1963) reported a case where the A coefficient at failure was 0.9 for a sample consolidated hydrostatically but was 1.8 when an essentially identical sample was consolidated with no lateral strain.

STRENGTH-WATER CONTENT RELATIONSHIP

Up to this point, strength has been examined in stress-stress diagrams. Such plots are the most useful because the usual input are stresses, e.g., overburden pressure, and the output are stresses, e.g., shearing strength. However, it may also be convenient to relate strengths to water content (void ratio, density, etc.) because water contents can easily be determined in the field. Water content is plotted versus the hydrostatic consolidation pressure for both drained and undrained tests on samples of remolded Champaign till in Fig. 28A. Clearly the relationship differs for normally consolidated and overconsolidated samples.

In Fig. 28B, the water content in the failure zone at failure are plotted against the compressive strengths and a unique relationship results for both drained and undrained tests, and for both normally consolidated and overconsolidated samples. A direct comparison of the water content-consolidation pressure, and water content-shearing strength relationships, is shown in Fig. 28C. The strength line is essentially parallel to the virgin consolidation line. If the R envelope is linear, then the relationship between $(1/2)(\sigma_1 - \sigma_3)_f$ and $\overline{\sigma}_{3c}$ is linear, i.e., $(\sigma_1 - \sigma_3)_f$ is some constant (usually about 0.6 for clays) times the consolidation pressure. For such a relationship, the plots of strength and consolidation pressure against a third variable (here water content) must be parallel in a semi-logarithmic diagram.

STRENGTH-EFFECTIVE NORMAL STRESS-WATER CONTENT SPACE

If the strength of a soil can be expressed as a function of effective stress, as in a Mohr-

Coulomb diagram, and as a function of water content, then it should be possible to plot strength data in strength/effective-normal-stress/water-content space. A problem develops because we can only view three axes. To reduce the complexity we choose to define:

$$\bar{p} = \frac{1}{3}(\bar{\sigma}_1 + \bar{\sigma}_3 + \bar{\sigma}_3) \tag{16.22}$$

and:

$$q = \frac{1}{2}(\sigma_1 - \sigma_3) \tag{16.23}$$

Consolidation curves are then plotted as $e - \bar{p}$ rather than say $e - \bar{\sigma}$, and Modified Mohr-Coulomb diagrams are plotted as $q - \bar{p}$. A $\bar{p} - q - e$ diagram is shown in Fig. 29. The failure points plot along the line marked "failure line in space", sometimes called the critical state line (CSL). The projection of the CSL onto the p-q plane produces a Modified Mohr-Coulomb diagram, marked in Fig. 29 as "failure envelope ($\bar{p} - q$)". Stress paths in space produce projections on the $\bar{p} - q$ plane similar to the stress paths previously plotted in Mohr-Coulomb diagrams (Figs. 10, 11. 14, 17, 18, and 27). For a sample that is normally consolidated initially, under a hydrostatic state of stress, the shearing stage starts with the specimen on the "virgin hydrostatic consolidation curve ($e - \bar{p}$)" in Fig. 29. Application of shearing stress (q) causes the stress path to move along a yield surface (not shown) and terminate on the CSL. The projection of the CSL on the $e - \bar{p}$ surface produces the $\bar{p} - e$ relationship at failure (line not shown in Fig. 29 but a line essentially parallel to the virgin hydrostatic consolidation curve). The "strength-void ratio relationship" (Fig. 29 is the projection of the CSL on the q-e surface. The diagram is too complicated in 3-D for general application but it provides a unifying concept between the modified Mohr-Coulomb diagrams and the strength-wafer content relationships.

The $\bar{p} - q - e$ diagram (Fig. 29) can be used as an approximation of actual shearing behavior of soils. It should not be assumed that shearing strength is a precise function only of $\bar{p}$ and e under generalized states of stress. The diagram does not conveniently show the post-failure loss in strength experienced by many soils, nor the effect of loading rate on strength, nor other effects as well. It is difficult to take an n-dimensional problem and reduce it to a form that can be plotted in three-dimensional space. Nevertheless, the diagram is found useful by some engineers.

Engineers who have become accustomed to using $\bar{p} - q - e$ space may choose to plot Modified Mohr-Coulomb diagrams of q vs $\bar{p}$ and consolidation data as e vs $\bar{p}$ or $\log \bar{p}$. If the slope of the $\bar{p} - q$ failure envelope is taken as $\bar{\psi}$ and the intercept as $\bar{d}$, in accord with previous usage in this book, and if we temporarily use:

$$R = \frac{\bar{\sigma}_1}{\bar{\sigma}_3} \tag{16.24}$$

then conversion to $\bar{c}$ and $\bar{\phi}$ requires use of the following equations:

triaxial compression: $$\sin(\bar{\phi}) = \frac{2}{3}\left(\frac{R+2}{R+1}\right)\tan(\overline{\psi}) \qquad (16.25)$$

triaxial extension: $$\sin(\bar{\phi}) = \frac{2}{3}\left(\frac{2R+1}{R+1}\right)\tan(\overline{\psi}) \qquad (16.26)$$

both: $$\bar{c} = \frac{\bar{d}}{\cos(\bar{\phi})}$$

STRAIN-RATE DEPENDENCY OF STRENGTH

Most soils, but particularly clays, have strengths that depend on the strain rate, both under undrained and drained conditions. Tests to study the influence of time on strength may be of the constant-load or constant-rate-of-deformation type.

Constant load tests are performed by applying a predetermined state of stress and measuring the strain as a function of time. For R and Q type drainage conditions (undrained), application of a small load leads to rapid deformation followed by negligible creep (curve 1 in Fig. 30). Application of a large load leads to failure at once (curve 3 in Fig. 30). Application of intermediate loads leads to rapid initial deformation, then a creep stage with strain rates decreasing with time, but sometimes to failure after a long period of creep (curve 2 in Fig. 30). Curves of applied stress versus time to failure can be used to indicate rate effects.

Casagrande and Wilson (1951) reported such a series of "undrained" (water must have migrated within the samples due to non-uniform stress states) tests using "undisturbed" samples of clay. Changes in strength per log cycle of time to failure were as shown in Table 16.2. Their times to failure ranged from 1 minute to 30 days (4.5 log cycles).

Table 16.2 Effect of Time to Failure on Undrained Compressive Strengths
(Casagrande and Wilson, 1951)

Soil	**Change in Strength per Log Cycle of Time to Failure, %**
Mexico City clay (soft)	3-6
Bearpaw Clay (clay-shale)	7-9
Oahe bentonite (clay-shale)	7-10
Cucaracha clay (clay-shale)	8-21

More conveniently, samples can be loaded at a constant rate of deformation and the strength reported as a function of strain rate. High speed constant-rate-of-deformation tests were reported by Casagrande and Shannon (1949), Cison and Parola (1968), and others. Data for a compacted clay of moderate plasticity are shown in Fig. 31.

If R is the fractional change in strength per log cycle of time to failure, and c_f and c_l represent the shearing strength in the field and laboratory, respectively, and t_f and t_l are the time to failure in the field and laboratory, then:

$$c_f = c_l\left(1 + R\log(\frac{t_l}{t_f})\right) \qquad (16.28)$$

If the times to failure in the laboratory and. field are 15 minutes and 6 months, respectively, and R is 0.05, then the field strength would be 80% of the laboratory strength.

Little information is available on the effect of strain rate on fully drained strengths because the minimum testing time for essentially full drainage is likely to be long, thus requiring the time for the longest test to be intolerably long, e.g., years. However, it appears that values of R may not be greatly different from the values found for undrained strength.

It appears that R may be small for sands, and, for soils in general, generally increases as the plasticity increases.

ANISOTROPY

Preceding considerations of shearing properties of soils have implicitly assumed that soils are isotropic, i.e., that shearing properties are identical for planes of any orientation passed through a point. It appears that most clays, and perhaps even coarser soils, are anisotropic. Soils may also be nonhomogeneous in that they may be composed of different materials. In the case of thinly stratified soils, the effects of inhomogeneities are similar in some regards to anisotropy.

An indication of anisotropy can be obtained by trimming samples at different angles and performing undrained compressive strengths. It is convenient to define 9 as the angle between the axis of the sample, and the vertical direction in the field, and R as the ratio of the strength for a sample at orientation 9 with the usual vertical sample. Sample data are shown in Table 16.3. Apparently, substantial variations in strength can occur for samples oriented differently.

Table 16.3 Influence of Sample Rotation on Undrained Strength of Clays.

Site	Soil Type	Reference	Rotation, deg	R
Waco	clay-shale	Wright and Duncan (1972)	0 45 60 90	1.00 0.40 0.40 1.36
Connecticut	soft clay	Healy(1967)	0 15 45 60 75 90	1.00 1.00 0.37 0.32 0.49 0.88
London	stiff clay (30 ft)	Ward, Marsland and Samuels (1965)	0 45 90	1.00 0.89 1.40
London	stiff clay (50 ft)	Ward, Marsland and Samuels (1965)	0 45 90	1.00 0.60 1.23

SENSITIVITY

Sensitivity is defined as the ratio of the undrained strength of an undisturbed soil to that of the same soil in a completely remolded condition at the same void ratio and temperature. Values of sensitivity can range from less than one to values too high to measure.

In the case of stiff fissured clays, the undrained strength may be low because of the presence of the fissures which have much lower shearing strengths than for the soil between the fissures. Remolding destroys these planes of weakness and strengthens the samples and leads to sensitivities between 0 and 1.

Typical soft clays have sensitivities ranging from two to ten. The sensitivities of such soils result, in part, from breaking down a soil structure that was originally developed to resist the consolidation pressure previously applied. Sensitivity also results from the rupture of cement that has formed spontaneously in nature at thecontacts between particles.

In the special case of leached marine clays, remolding may result in the clay becoming essentially fluid so the sensitivity is not subject to measurement (exceeds say 100).

RESIDUAL STRENGTHS

In a strain-controlled strength test it is possible to investigate strength after the peak strength has been reached. Imposition of large strains causes severe experimental problems (see later discussion of apparatus) and may make it difficult to track stresses at large strains. Stress-strain curves for a series of drained direct shear tests on samples of sand are shown in Fig. 32 (Casagrande and Leps, 1938). For these tests, the authors defined strain as the horizontal deflection divided by the thickness of soil involved in shearing. The loose sample decreased in volume during shear whereas the dense sample decreased in volume initially but then increased in volume during the rest of the test. At large strains it is possible that the samples have the same void ratio in the actual shear zone. Conditions at very large strains, where stresses are no longer changing, are given various names, e.g., the *ultimate condition*, *residual condition*, and *critical state*. The stresses in this condition may be essentially independent of the original density, overconsolidation ratio,....

A question exists as to whether engineering designs should be based on peak strengths or on the residual condition. This question is particularly important for one class of problems, viz., stability of slopes in stiff fissured clays and clay shales. It appears that deformations occurring in the field in the fissures is sufficient to reduce the average strength from the peak value toward the residual value. A Coulomb diagram for drained direct shear and triaxial shear tests is shown in Fig. 33 (Symons, 1967). Tests to evaluate the residual condition will be discussed in later chapters.

THIXOTROPY

If soft clays are remolded in the laboratory and then allowed to set at constant water content, they noticeably stiffen with time. If samples of remolded clay are molded into solid cylinders and sealed in membranes, they can be stored for varying periods of time, at essentially constant water content, and then their compressive strengths measured. The strengths are found to increase rapidly at first and then at a decreasing rate. Further, if, after a period of set-up time, a sample is remolded, the strength returns to the same strength it

had after first remolding, and then restarts an identical hardening process. This reversible hardening process at constant water content, temperature, and composition, is termed *thixotropy*.

Laboratory measurements show that the thixotropic strength gain results from the spontaneous development of negative pore water pressures. If the total stress is zero and the water pressure decreases then effective stress, and thus strength, increases with time.

The term "thixotropy" is often missused to describe time denpendent increases in strength, in the field, that are actually due to consolidation.

$\bar{\phi}$ CORRELATIONS

Measurement of $\bar{\phi}$ in the laboratory, for clays, is expensive. As a result, efforts have been made to correlate $\bar{\phi}$ with an index property. The relationship of (f) to plasticity index is shown in Fig. 34. Scatter is greatly reduced if the plot is restricted to remolded clays or to the residual value of $\bar{\phi}$ because then the effects of different soil structures is minimized.

$\bar{\phi}_S$ FOR SANDS

The S-type failure envelope of sand is concave towards the normal stress axis, i.e., the secant $\bar{\phi}_S$ (the secant $\bar{\phi}_S$ is the slope of the line drawn from the origin to a point on the failure envelope) decreases as the normal stress increases. Data for Molsand (from deBeer, 1967) are shown in Fig. 35. Clearly, $\bar{\phi}_S$ is less for loose sand than for dense sand.

INFLUENCE OF STRESS/STRAIN STATE

The shearing properties of soils are influenced by the overall state of stress in the sample, both during consolidation and during shear. During the consolidation stage, we are mainly concerned with the differences between properties of samples isotropically consolidated (convenient in the laboratory) and consolidated under conditions of no lateral strain (more typical in the field). This effect was discussed in Article 15.__.

Clays

For clays, many authors prefer to present strength data using c/p ratios (Art. 16.6). Bjerrum and Kenney (1967) presented the c/p ratios for normally consolidated samples of a Norwegian clay shown below:

triaxial compression	c/p=0.29
triaxial extension	c/p=0.13
direct simple shear (DSS)	c/p=0.18

The direct simple shear device is discussed in Article 16.__. The state of stress/strain in this device is similar to plane strain in that the principal strain in one direction is zero. In a more extensive series of tests using Boston Blue clay, Ladd and Foott (1974) found the following values:

Plane strain active	c/p=0.34
Triaxial compression	c/p=0.33
Direct simple shear	c/p=0.20
Plane strain passive	c/p=0.19
Triaxial extension	c/p=0.16

The plane strain tests were performed by using samples in the shape of rectangular prisms (all faces rectangles). An axial stress is applied (compression or extension) with one pair of opposite vertical faces subjected to a uniform pressure (as m triaxial tests) and the other pair subjected to stresses adequate to prevent strain perpendicular to those surfaces.

During consolidation of normally-consolidated sediments in the field, the vertical stress is the maximum principal stress and the horizontal stress is the minimum principal stress. Consolidation occurs under the soil particles have spontaneously shifted into positions such that they are braced against the field state of stress. Laboratory tests in which the vertical stress is the maximum principal stress (plane strain or triaxial compression) yield the largest strengths. Tests in which the principal stresses rotate 90degrees, and the soil is loaded in the opposite sense from the consolidation stage (extension tests) lead to a soil structure not braced to resist the imposed stresses and a lower strength results. The lower strengths are the result largely of the different pore water pressures set up during shear. For example, Koutsoftas (1981) found identical R failure envelopes for K_0 consolidated triaxial samples in compression and extension.

Sands

Much of the interest in influence of stress state on the properties of sands has involved plane strain conditions, simply because so many problems in geotechnical engineering are approximately plane strain problems. Examples include slope stability, retaining walls, and wall footings.

For sands, the soil is usually drained in the field for static loading conditions and thus the laboratory studies concentrate on S tests. The apparent angle of internal friction in plane strain compression is larger than for triaxial tests (Fig. 36). Cornforth (1964) found that the drained friction angle was about 4-5 degrees (10%) higher in plane strain, compared with triaxial compression, for dense sands, and that the difference tended to diminish as sands became looser. Leussink and Wittke (1964) found differences in $\bar{\phi}$ of up to 11 degrees for glass beads. Marachi et al. (1981) found that $\bar{\phi}$ was about 7 degrees higher for Monterey sand in plane strain for samples that were dense and at low confining pressure, but they found that the difference diminished both as the porosity increased (looser sands) and as the stress level increased. Initially, dense sands behave more and more like loose sands as the confining pressure increases so the observations of Marachi et al. are in keeping with other experience.

Strains at failure are consistently lower for plane strain compression tests as opposed to triaxial compression tests.

PARTIALLY SATURATED SOILS

Partially saturated soils contain both gas and liquid in the void spaces. Naturally occurring partially saturated soils range from arid soils with degrees of saturation approaching zero, to soft organic clays that contain a few gas bubbles. Compacted soils are always partially

saturated just after compaction in the field. Most of the data used in this section will have been collected for compacted soils but the principles developed will apply to naturally occurring soils as well. Because the physical properties of soils are conveniently explained using effective stresses, and the effective stresses are influenced by pore pressures, the discussion begins with a discussion of pore pressures in partially saturated soils.

Pore Water Pressures

It is convenient to think of partially saturated soils in two extreme, but common, cases.

In one case, the degree of saturation is above about 95, and the air is present in the soil as isolated bubbles. The water pressure is the same as it would have been if the soil had been saturated, and the pressure in the air bubbles is elevated.

In the second case, the degree of saturation is low enough that the air voids are essentially in full contact with each other and the water is thought of as being concentrated at the contact points between particles, plus some water spread out over the surface of the mineral particles. In the field, the pore air pressure is likely to be atmospheric (in this case) and the water pressure negative.

The interfaces between the pore water and pore air are curved because of the effects of surface tension. As a result, the pressure in the water is less than that of the pore air. For spherical air-water interfaces, the pressure difference is:

$$u_a - u_w = \frac{2T_S}{r} \qquad (16.29)$$

where u_a and u_w are the pore air and pore water pressures, respectively, T_S is the surface tension (about 75 dynes/cm), and r is the radius of curvature of the interface. For very small radii, the water pressure may be much less than the air pressure. Equation16.29 breaks down for clays but it serves current needs adequately (see Olson and Langfelder, 1965, for a more rational explanation of pore pressures).

Pore water pressures between 0 and about -10 psi can be measured more or less in the same way that positive pore water pressures are measured. More negative pore water pressures can be measured using an axis translation technique (Olson and Langfelder, 1965) or psychrometers (Daniel et al., 1981). Pore water pressures for a compacted clay are plotted against the compaction water content in Fig. 37 for several clays. Clearly, for partially saturated compacted soils near the ground surface, the magnitude of the pore water pressure can be much larger than that of the total stress, and thus the pore water pressure exerts an important influence on the physical properties of such a soil.

Effective Stresses in Partially Saturated Soils

The presence of two pore fluids invalidates Terzaghi's equation for effective stress (Eq. 1.1). A simple alternative equation was offered by Bishop (1955):

$$\bar{\sigma} = \sigma - \chi u_w - (1-\chi)u_a \qquad (16.30)$$

where u_w and u_a are the pore water and pore air pressures, respectively, and χ is an empirical coefficient that is one for a saturated soil, and zero for a dry soil. For practical purposes,

numerical values for χ drop to negligible values for degrees of saturation below about 90. Thus, a soil that contains only a small amount of water, may have a very negative pore water pressure but χ is so small that the effective stress caused by the negative pore water pressure is also small. For soils with only a few isolated air bubbles, the negative pore water pressure pulls the particles together essentially throughout the soil mass and χ is essentially one. For soils with continuous air voids, the water will generally coat the soil particle surfaces but be concentrated at the interparticle contacts. The negative pore water pressure at the contacts thus pulls the particles together and generates the effective stress. Highly negative pore water pressures should produce large effective stresses, but if the water area around each particle contact is small (low degree of saturation) then the force at the contact is small (corresponds to a low value for the empirical factor χ). Experiments show that Eq. 16.30 cannot be valid in general and that a much more complicated (and thus not very useful) approach is required. We will use the simple equation but not extend its application to a point where problems develop.

Q-Tvpe Failure Envelopes

A series of failure envelopes for a compacted clay of moderate plasticity are shown in Fig. 38. For this clay, the optimum water content was 15. For specimens compacted at water contents above optimum, the failure envelopes are essentially horizontal. For specimens compacted at water contents significantly less than optimum, the envelopes are concave downwards but have finite values of ϕ_Q even at a confining pressure of 1000 psi.

An explanation of the shape of the envelopes utilizes effective stresses. For saturated soils, the pore water is much less compressible than the framework of mineral particles so essentially all of an increment of applied stress goes into the pore water (B=1). The resulting negligible change in effective stress causes a negligible change in strength and the Q-type failure envelope of saturated soils is essentially horizontal. For partially saturated soils, the pore air is highly compressible. Application of a confining pressure causes the air to compress, and thus the sample to decrease in volume, and thus the effective stress to increase. The increasing effective stress leads to a finite value of ϕ_Q. However, when the pore air pressure increases, some of the pore air dissolves in the pore water, increasing the degree of saturation. Thus, if the total stress on a sample is slowly increased, the sample gradually becomes increasingly saturated, and the failure envelope becomes flatter.

This explanation can be quantified slightly through use of the B coefficient. Because of the presence of two pore fluids, it becomes necessary to use two coefficients, B_a for the air and B_w for the water. Values of B_w are plotted against the initial degree of saturation for samples of a compacted clay, in Fig. 39. For degrees of saturation less than about 95, it is clear that only small water pressures develop when a sample is subjected to an increase in the hydrostatic total stress, and thus most of the applied stress goes into the soil structure and causes an increase in strength. For higher degrees of saturation, B_w approaches one, applied stresses go into water pressure, and ϕ_Q approaches zero.

The range in applied stresses in Fig. 38 is more than will been countered for most engineering projects. For ranges in stress below about 100 psi, the failure envelopes can often be approximated as straight lines. Typical data for c_Q and ϕ_Q for a compacted clay are shown in Fig. 40. The optimum water content for this clay was 19%.

R and S Envelopes

It is not common to perform R and S-type tests, deliberately, onpartially saturated samples

and thus the discussion of such caseswill be brief.

Air drained samples If the soil is initially to be consolidated, there are two options. In the first, the drains are opened to the atmosphere and the sample might be said to be air drained because the air pressure at the drainage boundary is set at some predetermined constant value, typically one atmosphere absolute, and no water is made available to the sample.

If the degree of saturation is high and the applied stress is large enough to cause drainage, then the pore water drains just as for saturated samples. The subsequent R and $\overline{R}$ envelopes are the same as for saturated specimens except for cases where negative pore water pressures tend to develop. In such cases, no water can be sucked into the sample so, instead, the pore air expands freely, allowing volume change, and the R tests resemble an S test. For S tests, if positive pore water pressures develop, the test is identical to that for a saturated sample in that the water can drain out of the sample. If negative pore water pressures tend to develop, no water can be drawn into the sample but the air bubbles expand freely and the sample again behaves as if it were water drained.

If the degree of saturation is lower so the air voids are interconnected, then consolidation involves dissipation of excess pore air pressures. Pore water pressures are negative and thus no water drainage occurs. Positive pore water pressures are unlikely to develop during shear either. $\overline{R}$ tests are not feasible because of the difficulty in defining effective stresses even when the pore air and pore water pressures are known. R tests generally tend to act as if they were S tests because the pore air expands and contracts so freely that it allows volume change to occur. However, the negative pore water pressure that existed at the beginning of shear tends to remain throughout the test and causes an increased effective stress and thus increased strength compared with say tests on saturated samples. In air drained tests, the initial negative pore water pressures tends to remain during shear.

Water-drained tests The term water drained is used to indicate that the drainage values are opened to a line full of water. If positive pore pressures develop when the confining pressure is applied, then drainage occurs naturally. If negative pore water pressures exist under the confining pressure, then water is sucked into the specimen and the degree of saturation tends to rise to some value in the range of 90-100%, depending on whether or not pore air is allowed to escape from one end of the specimen as water enters the other end. In any case, at the end of the consolidation stage, the sample has a high degree of saturation, but not 100%.

For R and $\overline{R}$ tests, if positive pore water pressures are generated, then the entrapped gas bubbles compress, allowing a reduction in void ratio, and the sample tends to behave as if it were a drained test if the soil structure is incompressible and more as an undrained test if the soil structure is highly compressible. If negative pore water pressures start to develop, the entrapped gas bubbles expand freely and the soil acts as if it were drained.

For S tests, the sample behaves essentially as if it were saturated.

Closing comments The number of options developing with tests on partially saturated samples is such that most laboratories choose either to saturate specimens before testing, if they will be under the water table in the field, or run the simple Q tests. $\overline{R}$ tests with negative pore water pressures are too difficult arid expensive to perform for most laboratories and projects.

MULTI-STAGE TESTING

Most failure envelopes are defined using one shear test per sample. Scatter thus results from the fact that no two samples are identical. An alternative procedure is to shear a sample just to the point of failure under one confining pressure, then raise the confining pressure and shear to failure again, and continue the process for as many stages as can be accomodated before the accumulated strains become excessive. The procedure seems to have been originated by Taylor (1950) and rediscovered later by others, e.g., Fleming (1952). In the case of Q tests at constant rate of deformation, the loading process may be continuous with the confining pressure raised incrementally at appropriate points. For R and S tests, the shearing stage is stopped and the sample consolidated under the new state of stress, and shearing begun again. Calculation of sample areas becomes difficult for large strains so this procedure typically can be used for only two or three stages.

The multistage testing procedure works well only if each stage is stopped precisely at the point of failure, or perhaps slightly before failure. If a shear plane forms, then subsequent shear tests yield strengths lower than would have been obtained using a fresh identical sample.

It should be noted that a stage test typically defines a single failure envelope rather well (minimal scatter). It does not define the properties of soil strata in the field with such precision, and indeed may even mask the real variation in properties if only a few tests are performed. The advantage of the test is that it allows more data for a relatively minimal incremental cost.

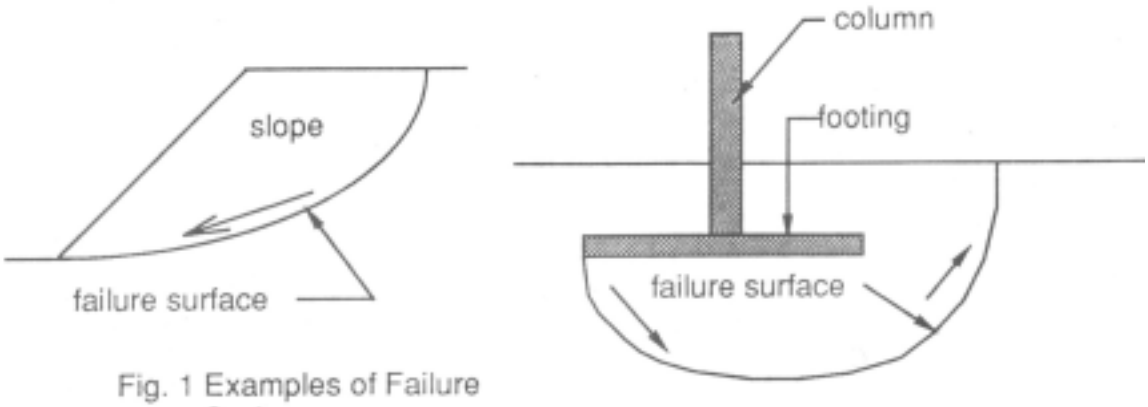

Fig. 1 Examples of Failure Surfaces

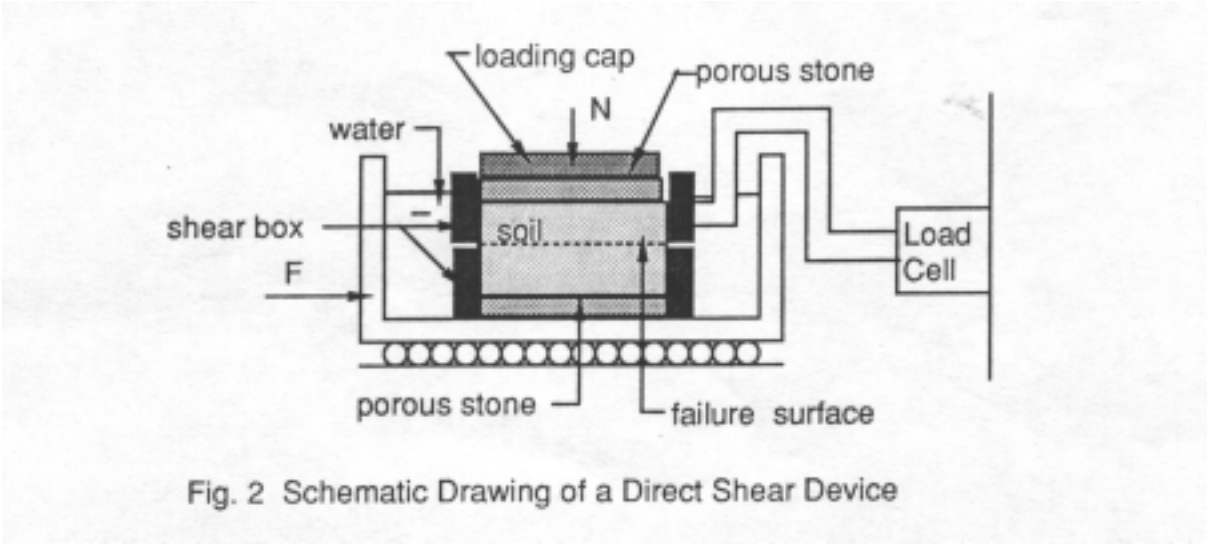

Fig. 2 Schematic Drawing of a Direct Shear Device

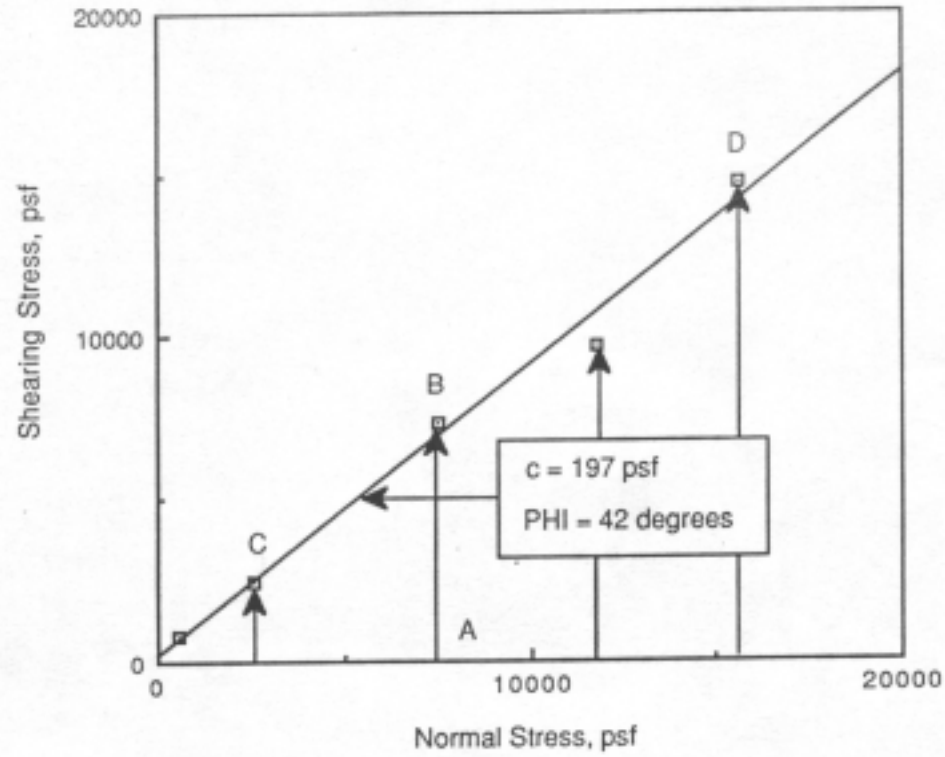

Fig. 3 Coulomb Diagram for a Dense Well-Graded Sand in Direct Shear

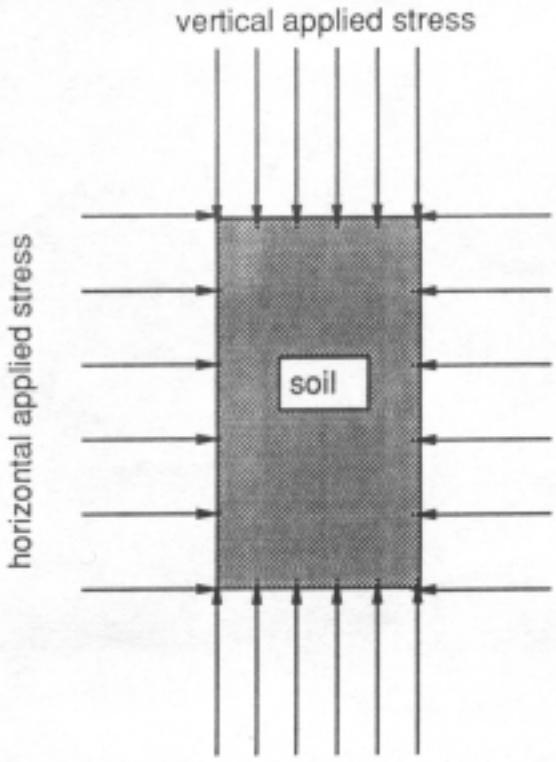

Fig. 4 Stresses Applied to Sample in the Triaxial Device

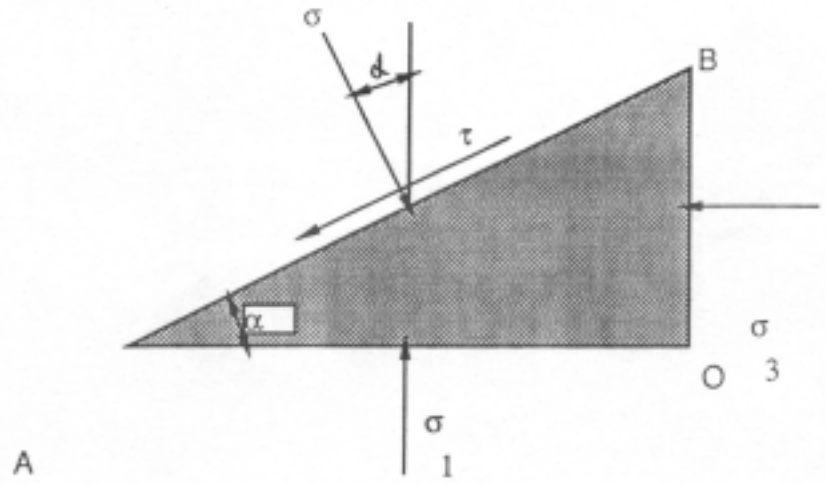

Fig. 5 Differential Element Used to Develop Equation for Mohr's Circle

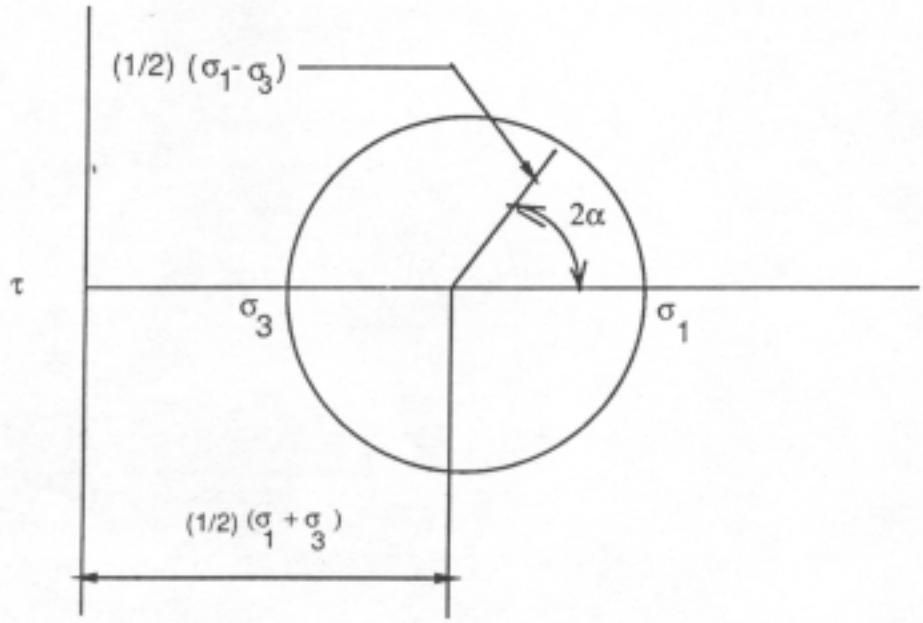

Fig. 6 Coordinates used in a Mohr Circle

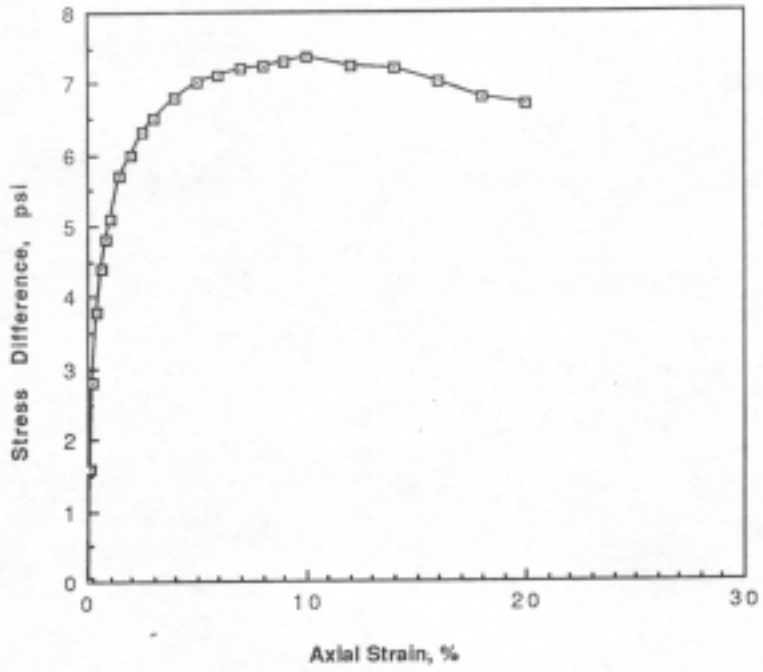

Fig. 7 Stress-Strain Curve for a Triaxial Compression Test

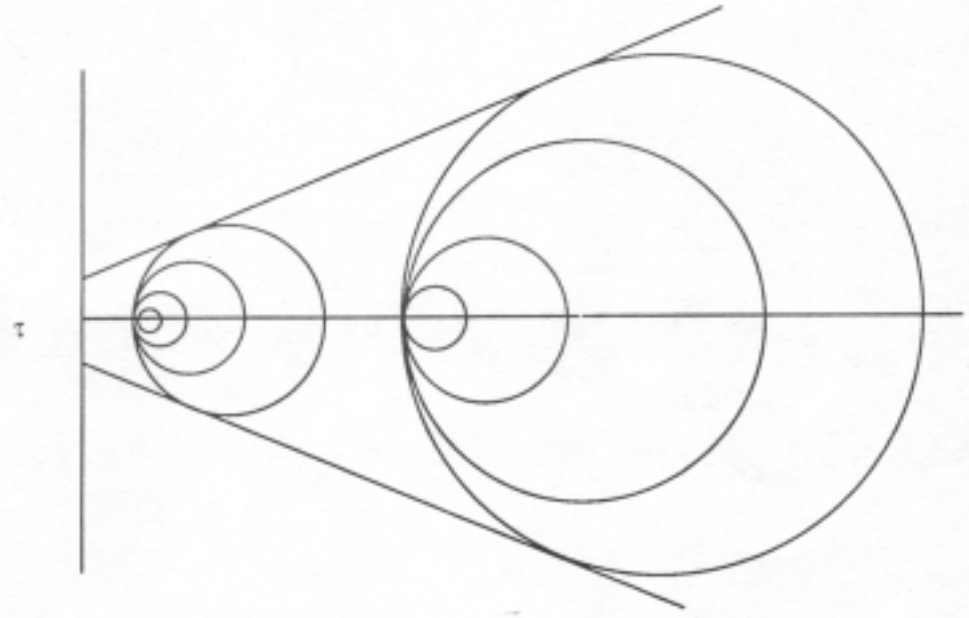

Fig. 8 Expanding Mohr Circles during Triaxial Compression Tests

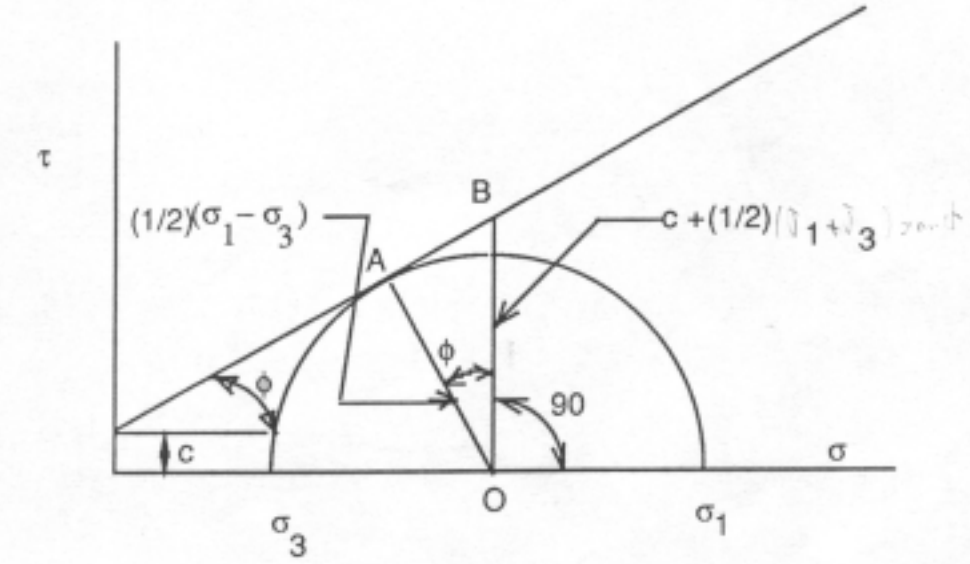

Fig. 9 Stress Relationships for Mohr Circles

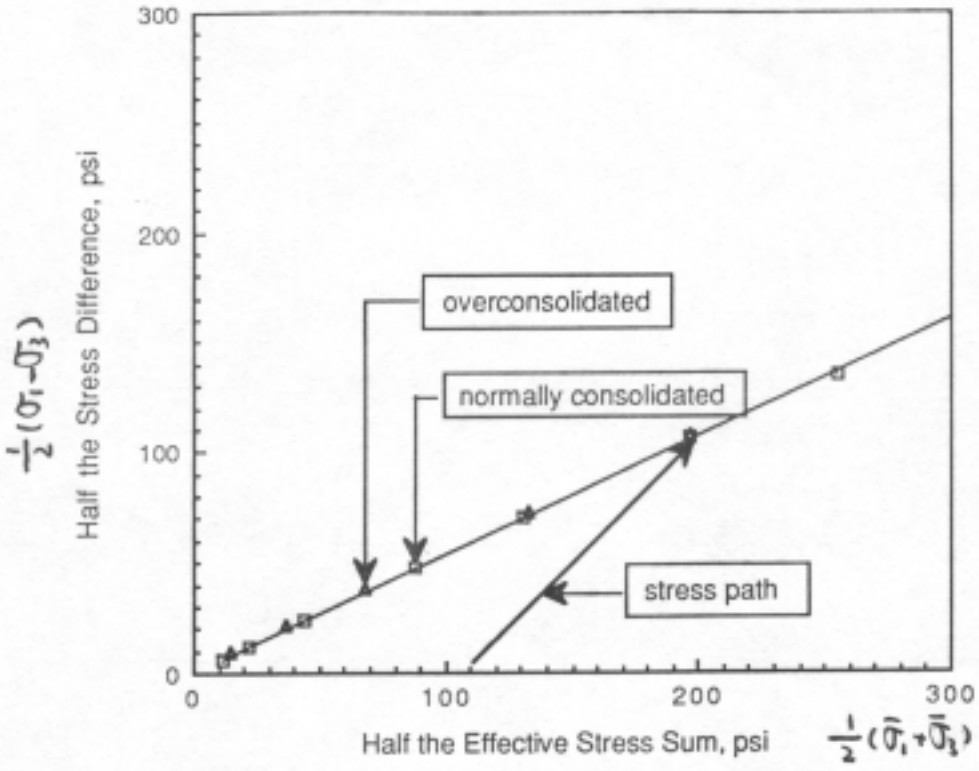

Fig. 10 Modified Mohr-Coulomb Diagram for Drained Triaxial Compression Tests on Normally Consolidated and Overconsolidated Champaign Till

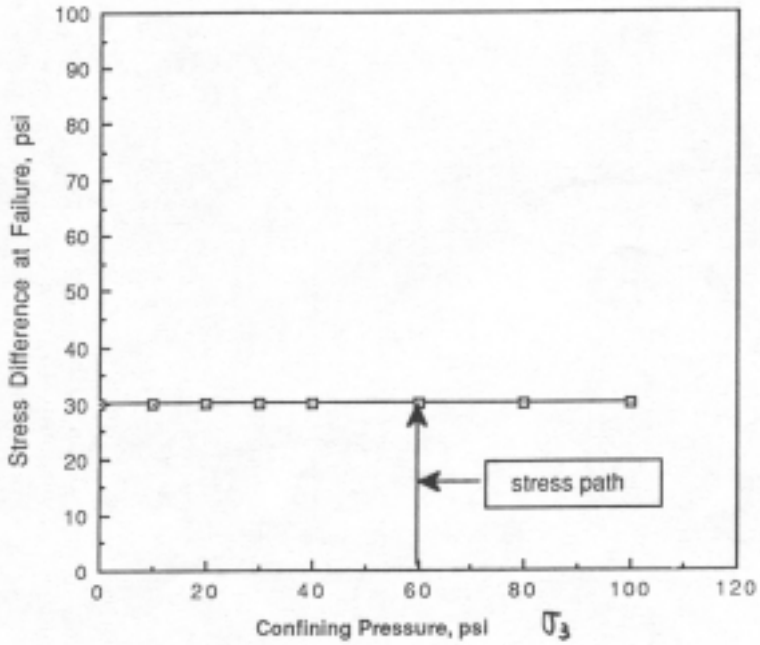

Fig. 11 Modified Mohr-Coulomb Diagram for a Series of Q-Type Triaxial Compression Tests on Samples of Saturated Soil

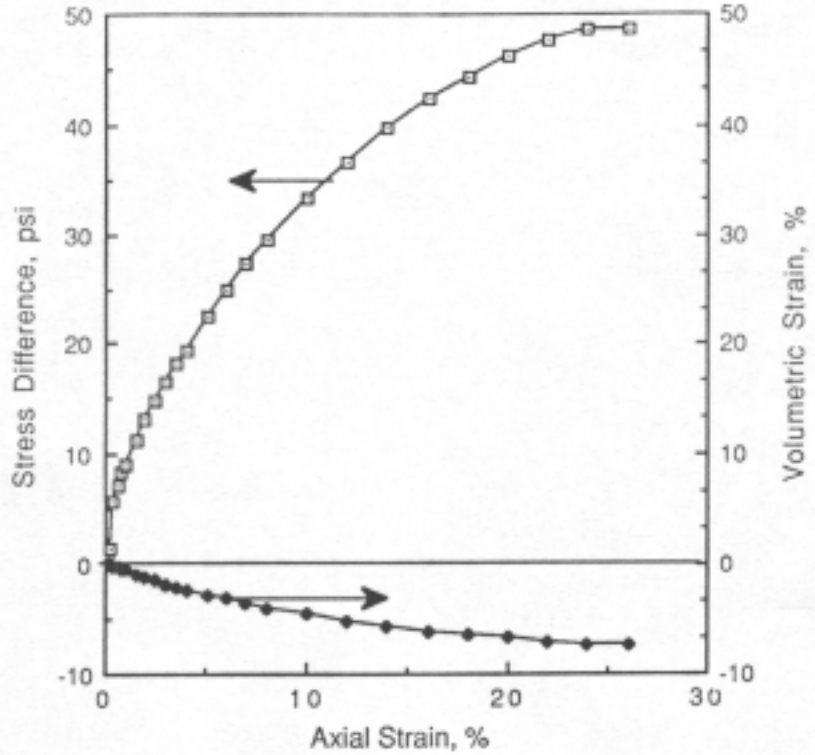

Fig. 12 Stress-Strain Curves for an S-Type Triaxial Compression Test on a Sample of Kaolinite Consolidated to 80 psi

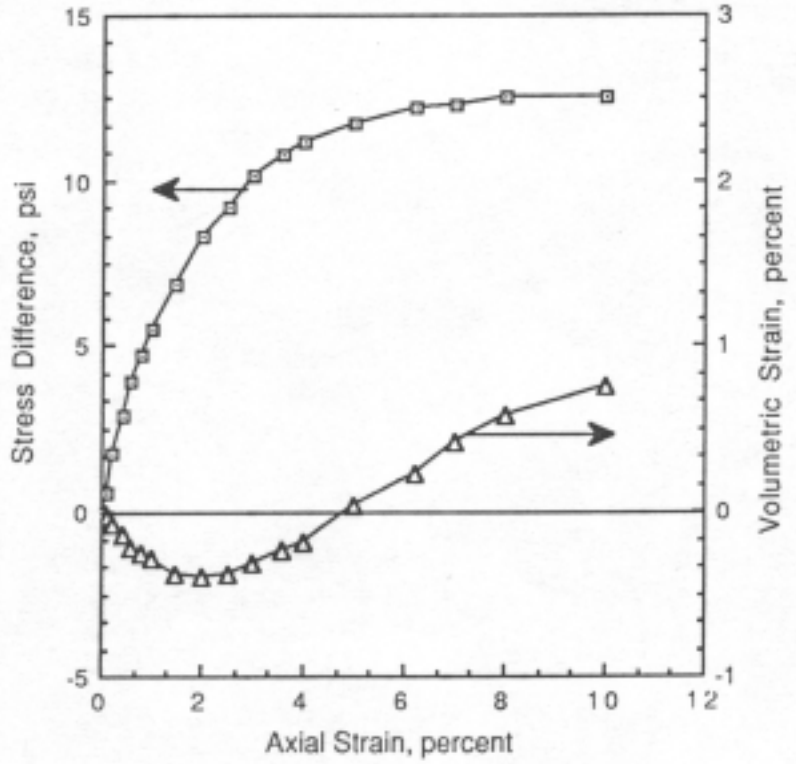

Fig. 13 Stress-Strain Curve for Drained Triaxial Compression Test on a Sample of Kaolinite that was Consolidated to 120 psi and then Rebounded to 5 psi

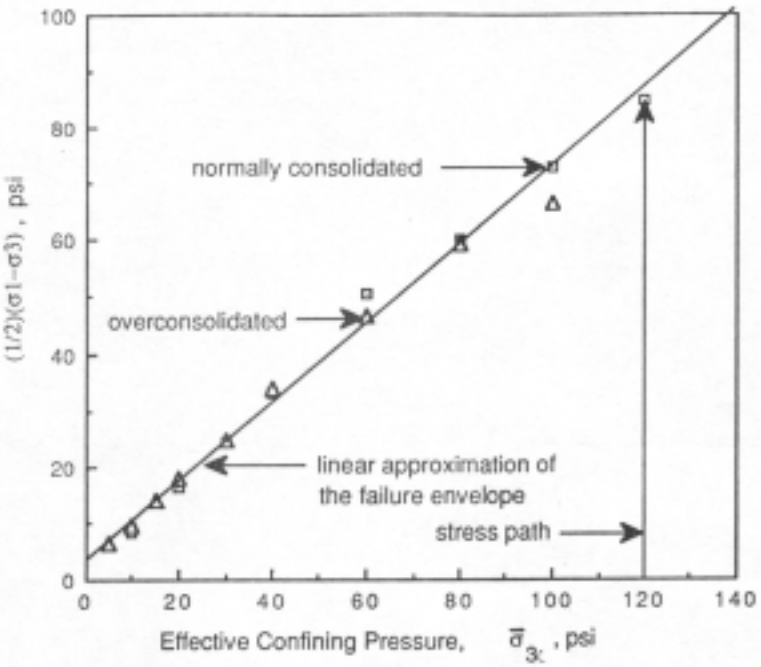

Fig. 14 Modified Mohr-Coulomb Diagram for Drained Triaxial Compression Tests on Samples of Kaolinite

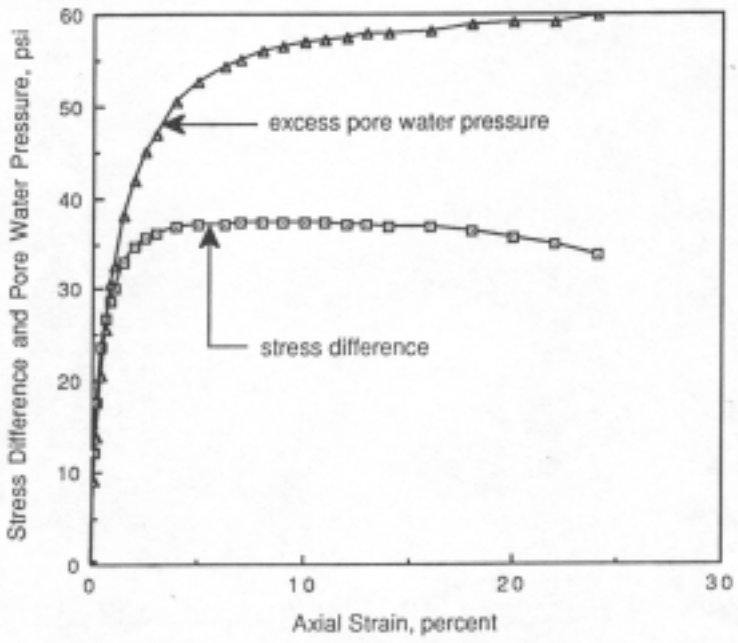

Fig. 15 Stress-Strain Curves for R' Triaxial Compression Test on a Sample of Kaolinite Normally Consolidated to 80 psi Prior to Shear

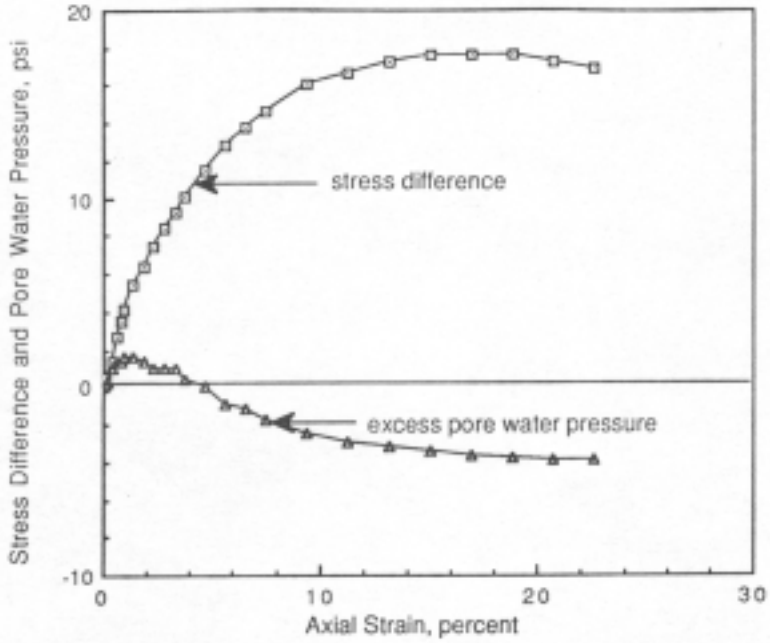

Fig. 16 Stress-Strain Curves for R' Triaxial Compression Test on a Sample of Kaolinite that was Consolidated to 120 psi and Rebounded to 5 psi Prior to Shear

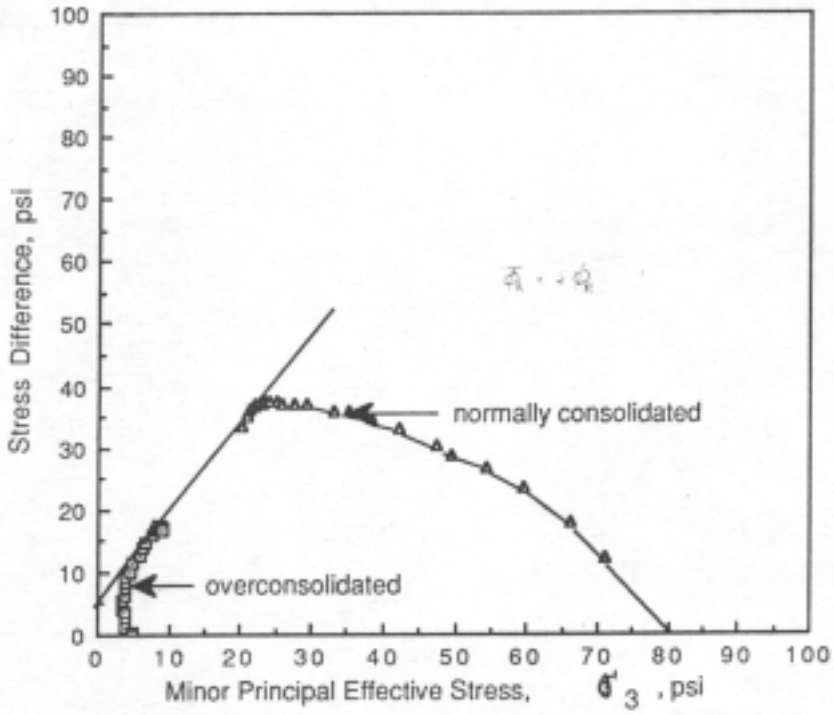

Fig. 17 Stress-Path Curves for R' Tests on Normally Consolidated and Overconsolidated Samples of Kaolinite

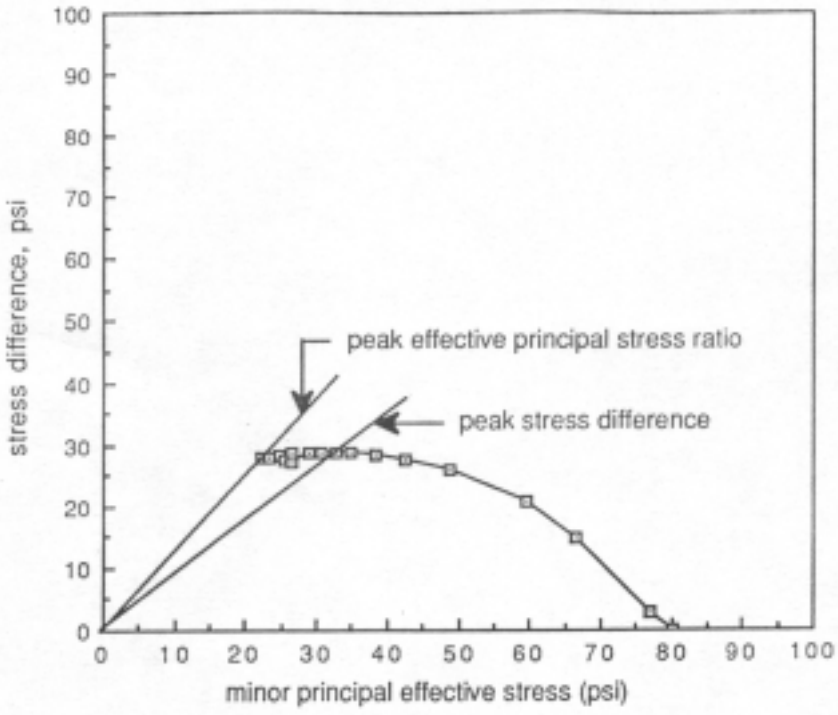

Fig. 18 Stress Path Curve for an R' Triaxial Compression Test Showing the Effect of using Two Failure Criteria

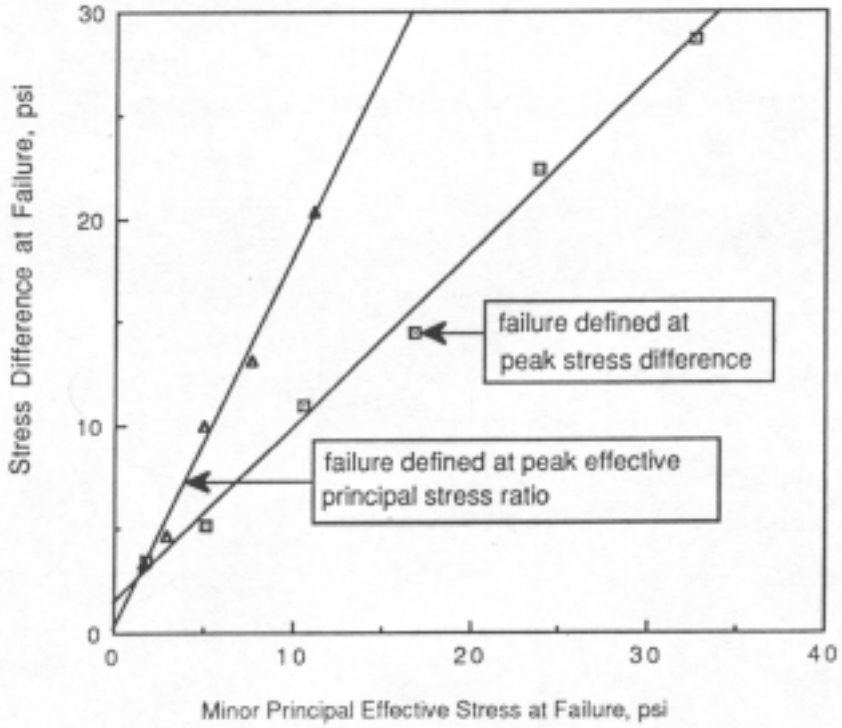

Fig. 19 Failure Envelopes of a Kaolinite Defined using Two Failure Criteria for R' Triaxial Compression Tests

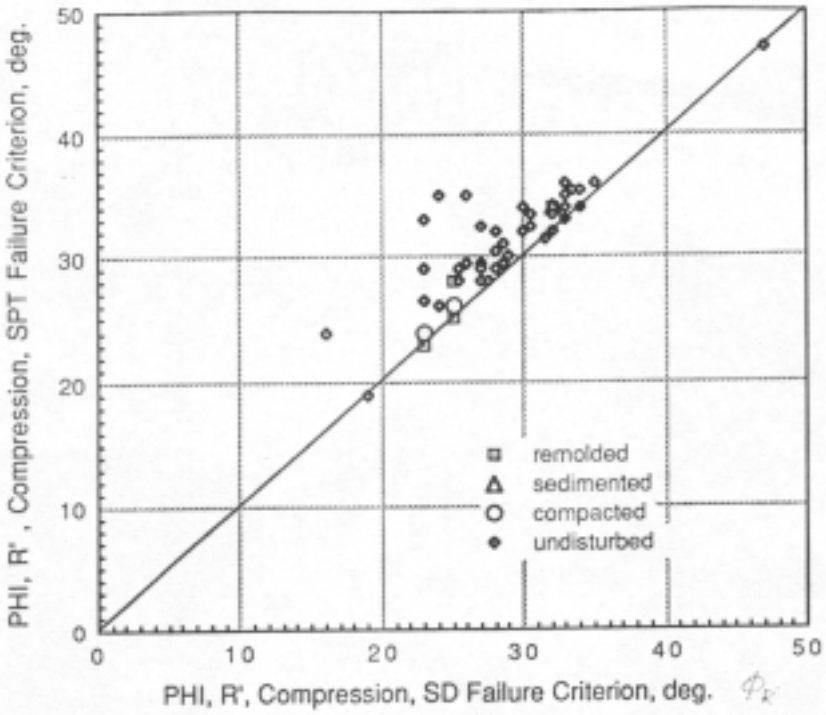

Fig. 20 Comparison of Effective Angles of Internal Friction from Undrained Triaxial Compression Tests, using Two Different Failure Criteria

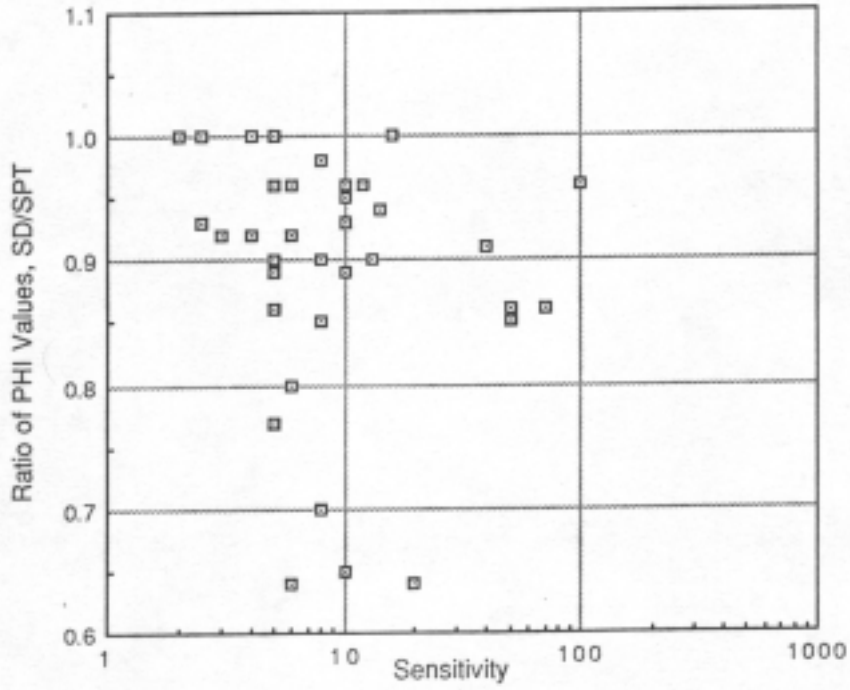

Fig. 21 Influence of Sensitivity on the Ratio of PHI Values at the Peak SD and SPT Failure Criteria for R' Triaxial Compression Tests

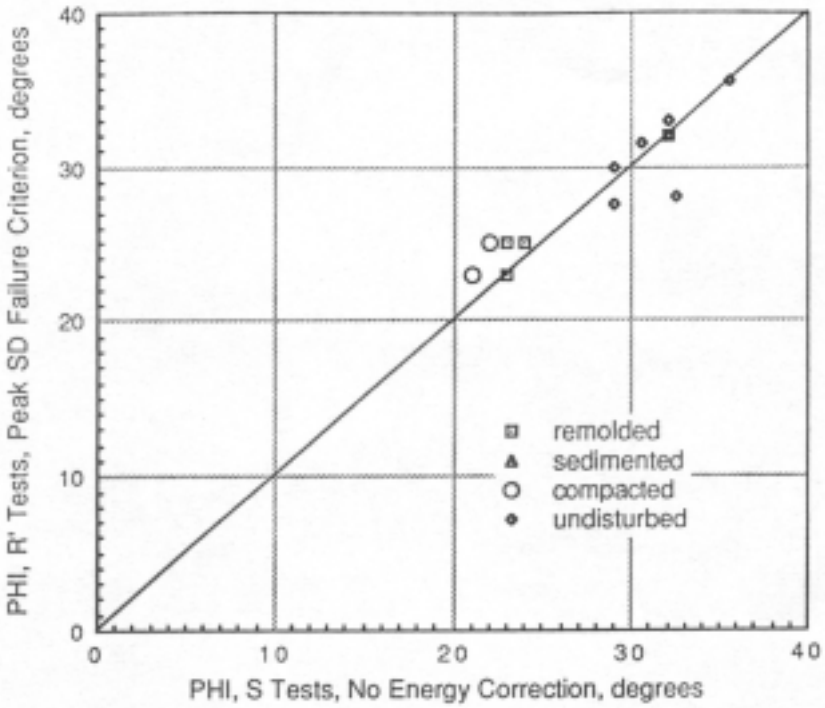

Fig. 22 Comparison of Effective Friction Angles in R' (Peak SD) and S (no energy correction) Triaxial Compression Tests

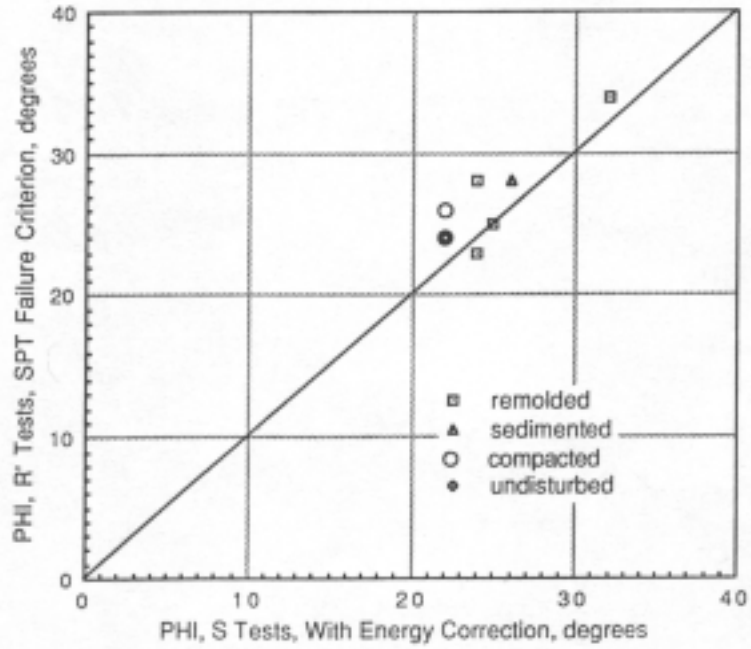

Fig. 23 Comparison of Effective Friction Angles for R' (SPT) and S (with energy correction) Triaxial Compression Tests

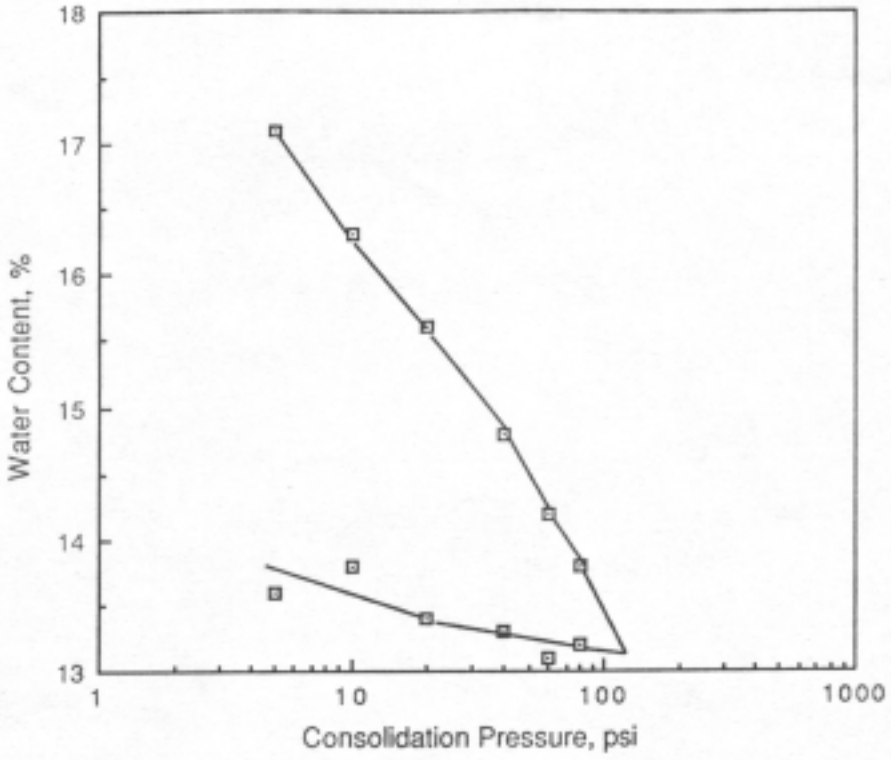

Fig. 24 Consolidation Curve for Samples of Champaign Till

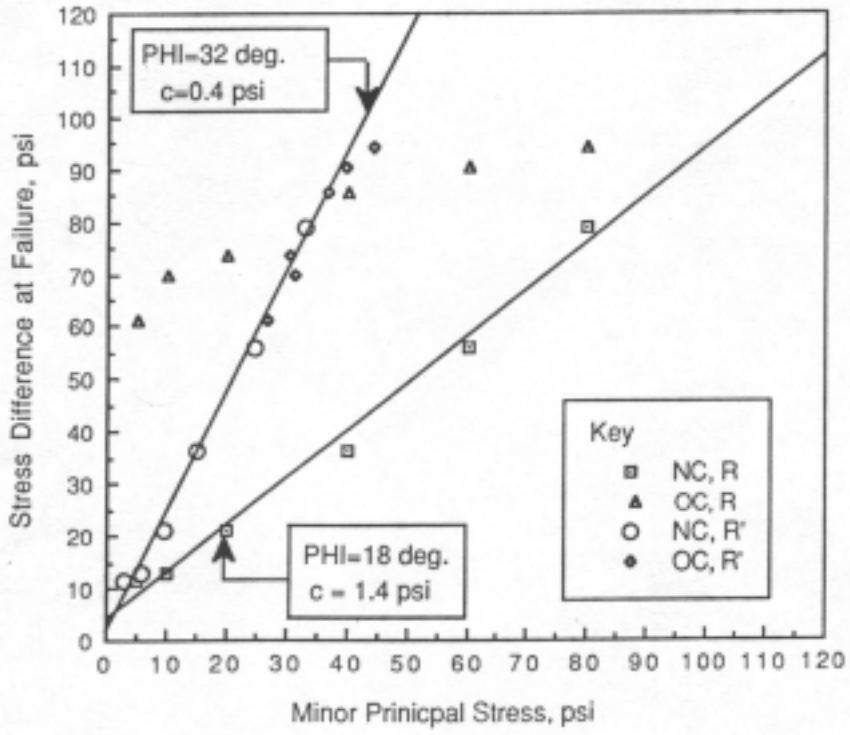

Fig. 25 Comparison of Modified Mohr-Coulomb Diagrams for Normally Consolidated and Overconsolidated Samples of Champaign Till in R and R' Diagrams

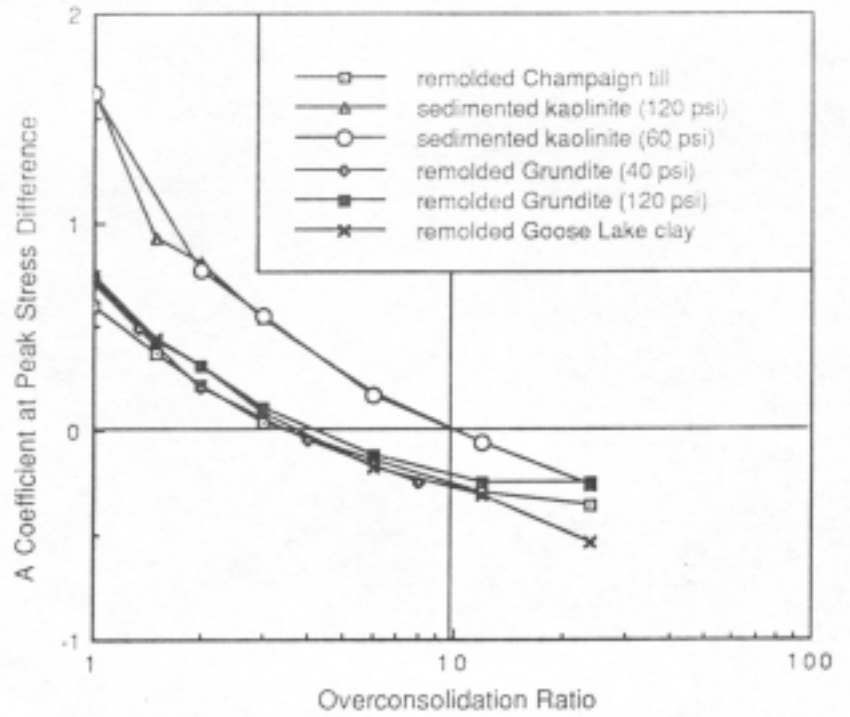

Fig. 26 Influence of Overconsolidation Ratio on Skempton's A Coefficient at the Peak Stress Difference

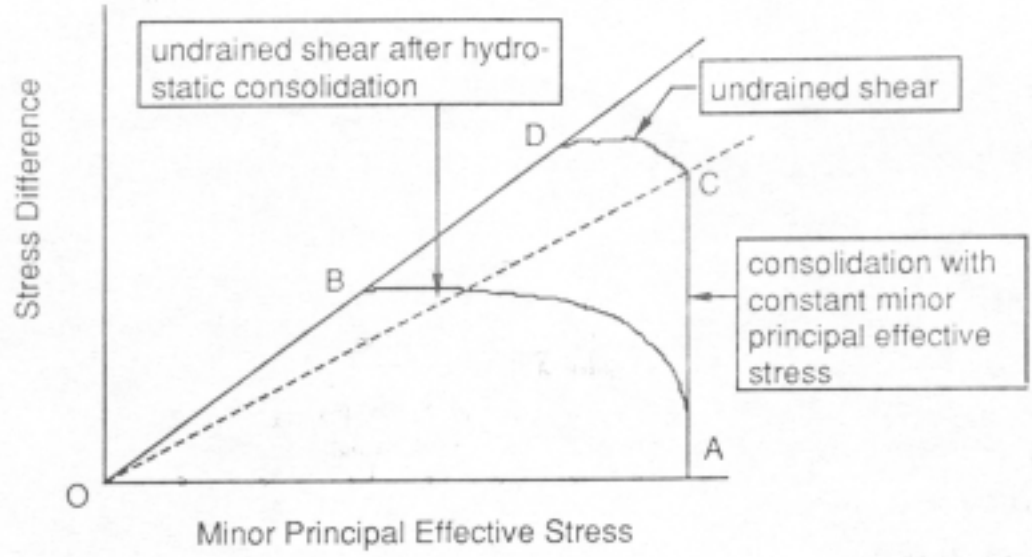

Fig. 27 Stress Path Curves for Undrained Compression Tests on Normally Consolidated Samples After Hydrostatic (Path AB) or Constant Minor Principal Effective Stress (ACD) Consolidation

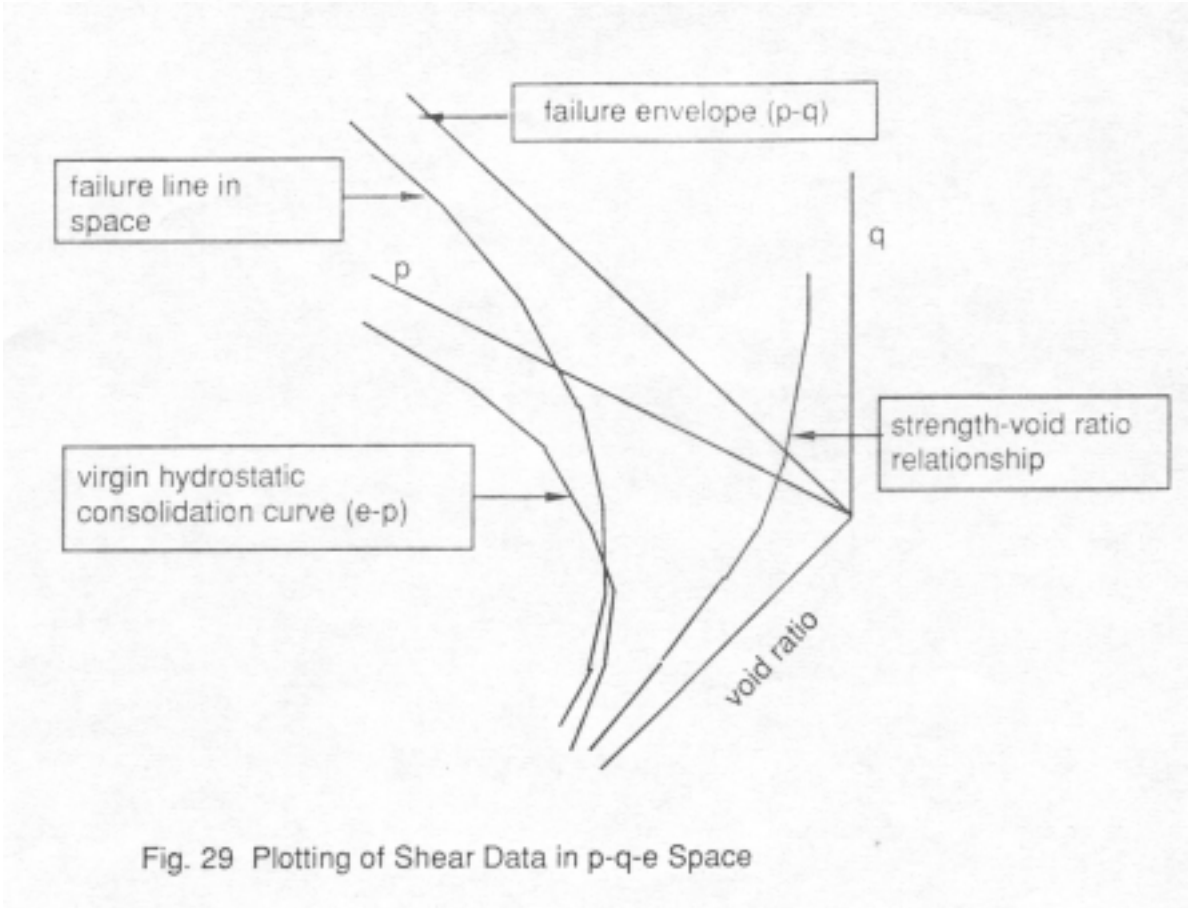

Fig. 29 Plotting of Shear Data in p-q-e Space

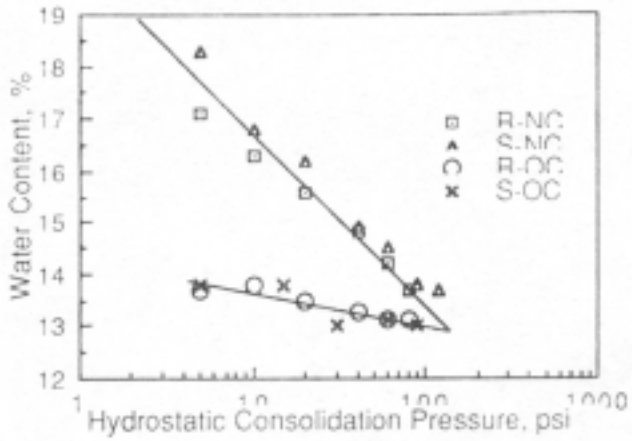

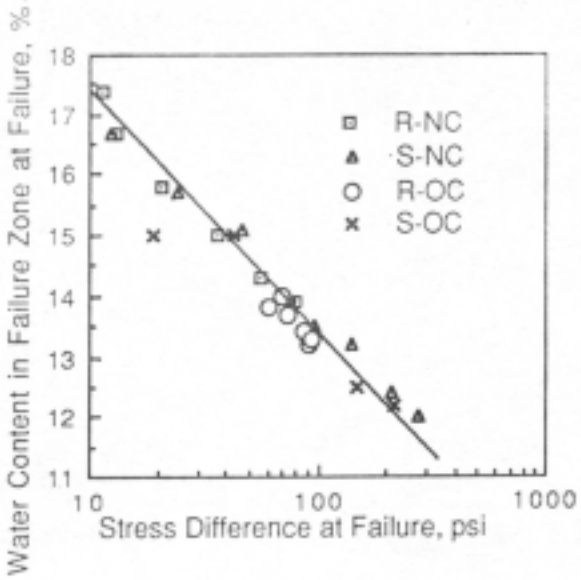

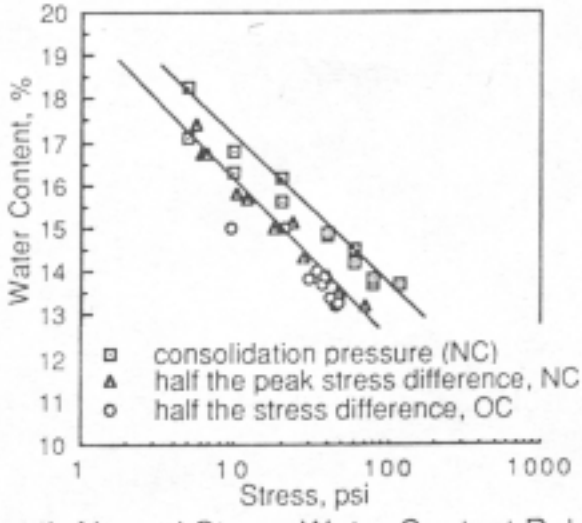

Fig. 28 Strength-Normal Stress-Water Content Relationships for Champaign Till

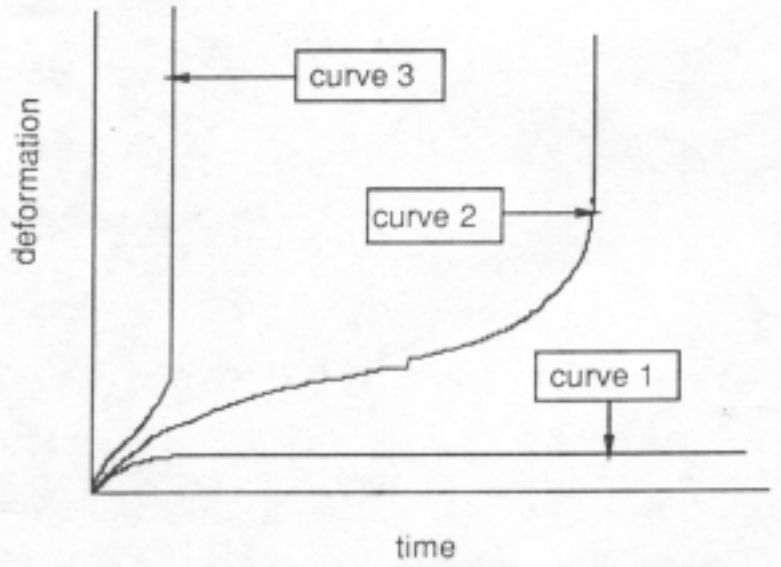

Fig. 30 Time-Deformation Curves for Constant-Load Tests on Samples of Soil

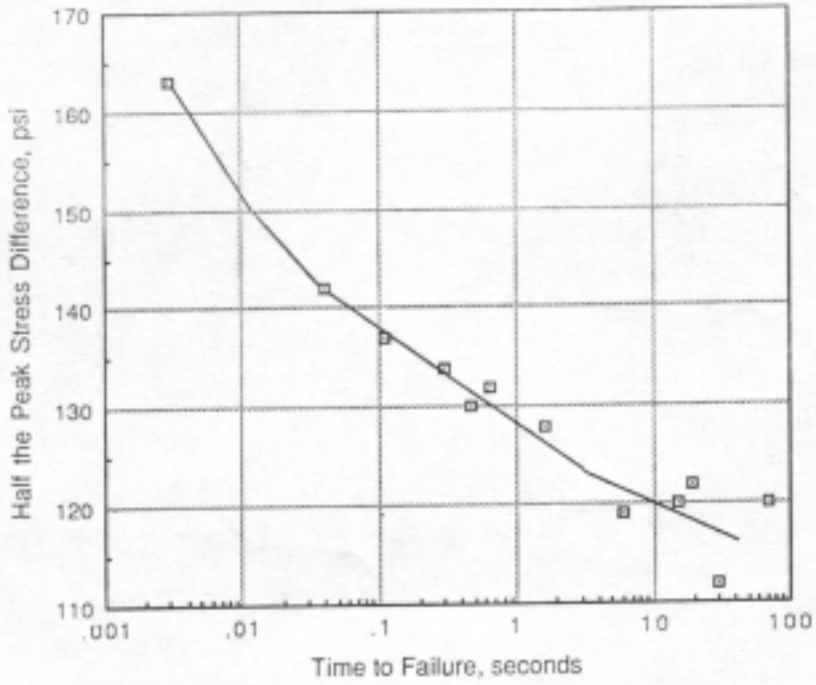

Fig. 31 Influence of the Time to Failure on the Shearing Strength of Compacted Goose Lake Clay at a Confining Pressure of 114 psi

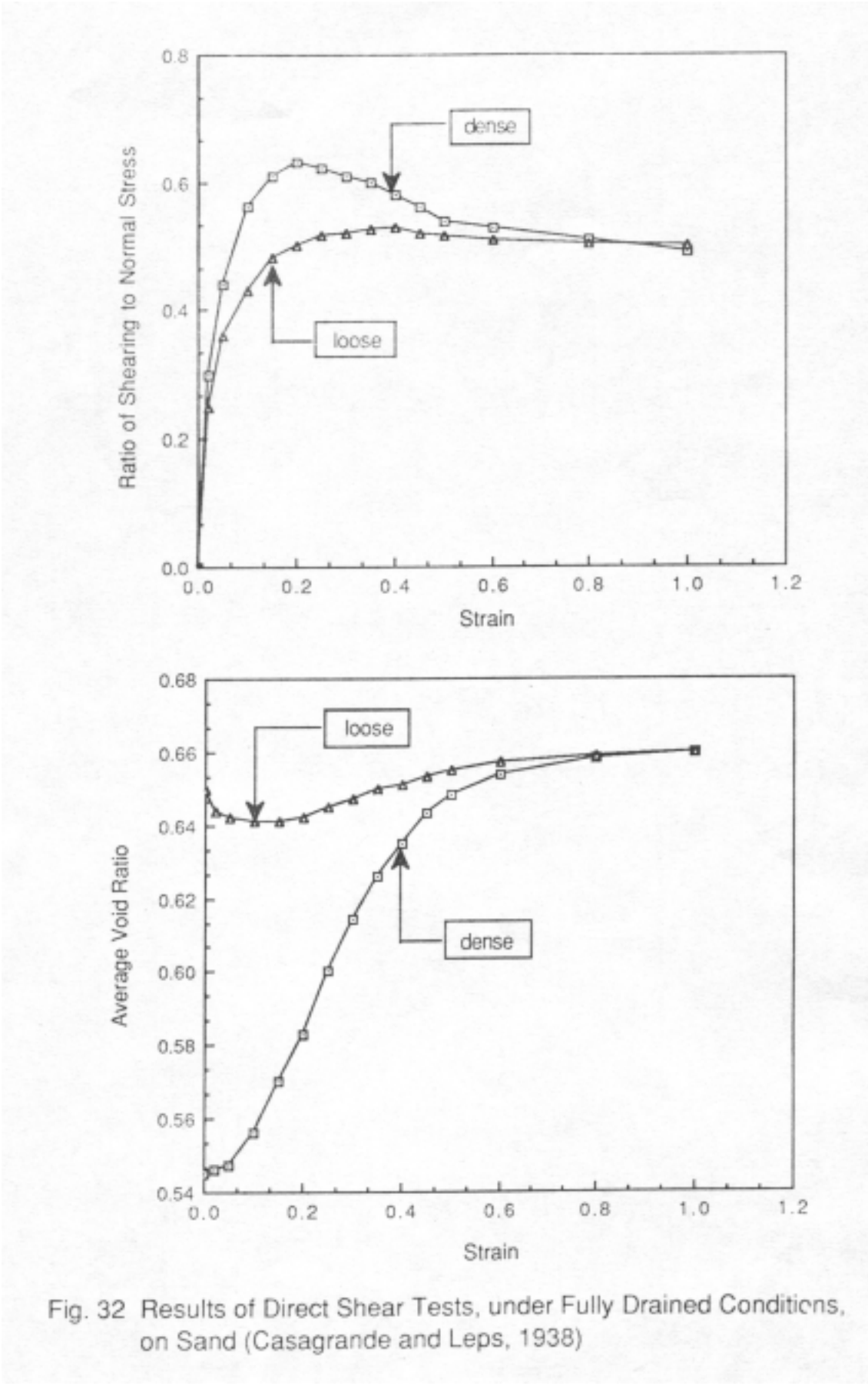

Fig. 32 Results of Direct Shear Tests, under Fully Drained Conditions, on Sand (Casagrande and Leps, 1938)

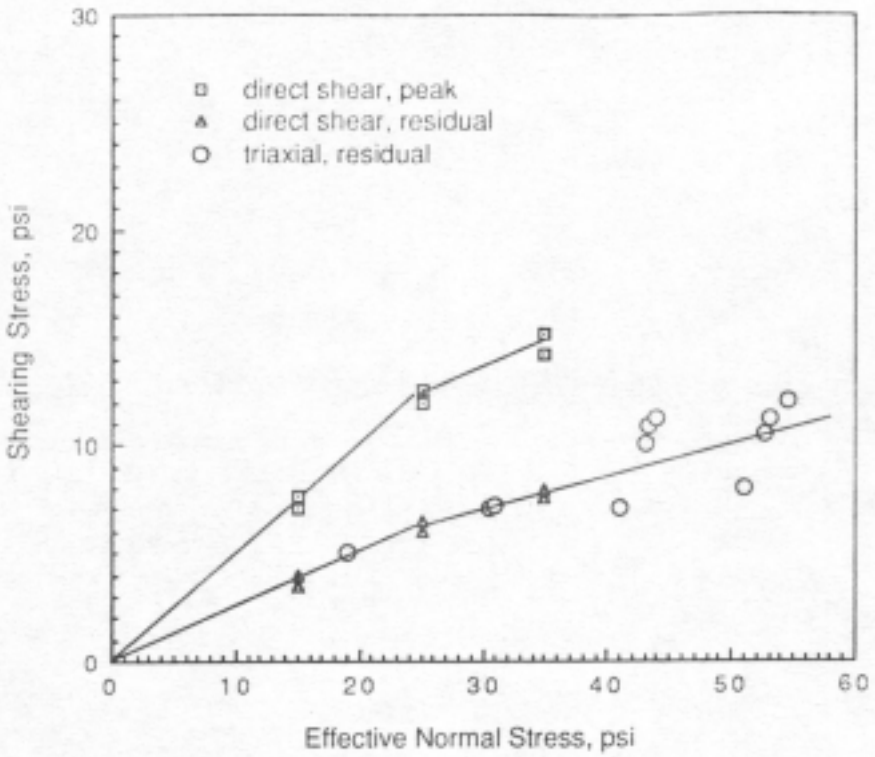

Fig. 33 Failure Envelopes at Peak and Residual Conditions in Direct and Triaxial Shear (Symons, 1967)

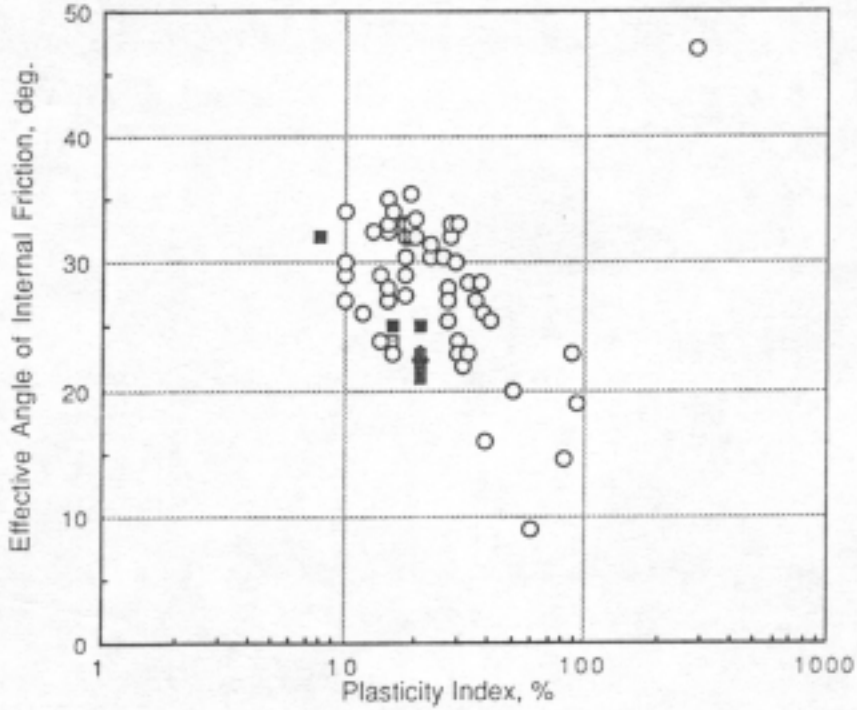

Fig. 34 Relationship Between Effective Friction Angle and Plasticity Index (Key: open box=remolded, filed box=compacted, open circle=undisturbed, open triangle=sedimented)

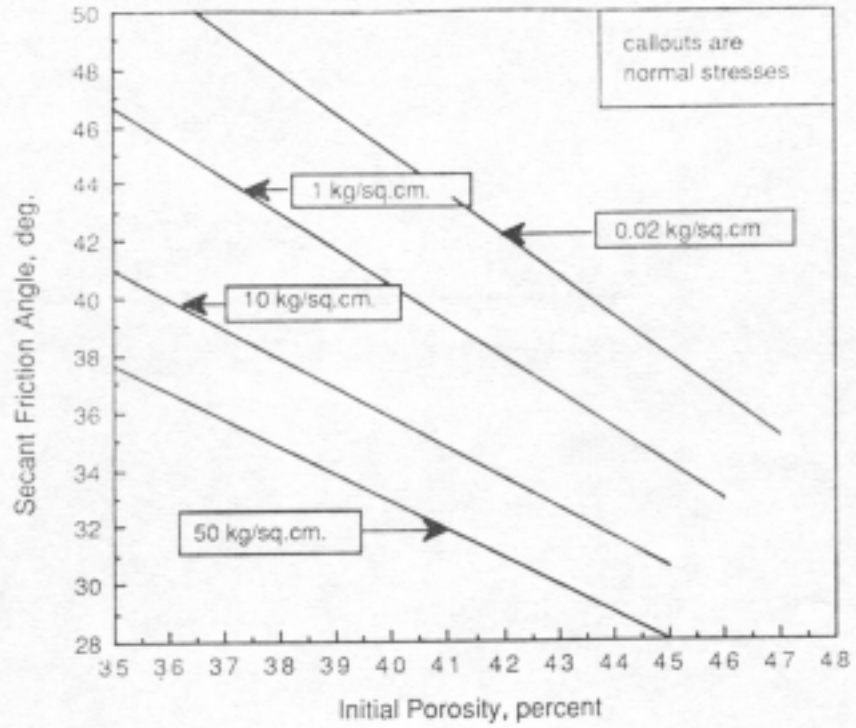

Fig. 35 Influence of Initial Porosity and Confining Pressure on the Effective Triaxial Friction Angle of Molsand (deBeer, 1967)

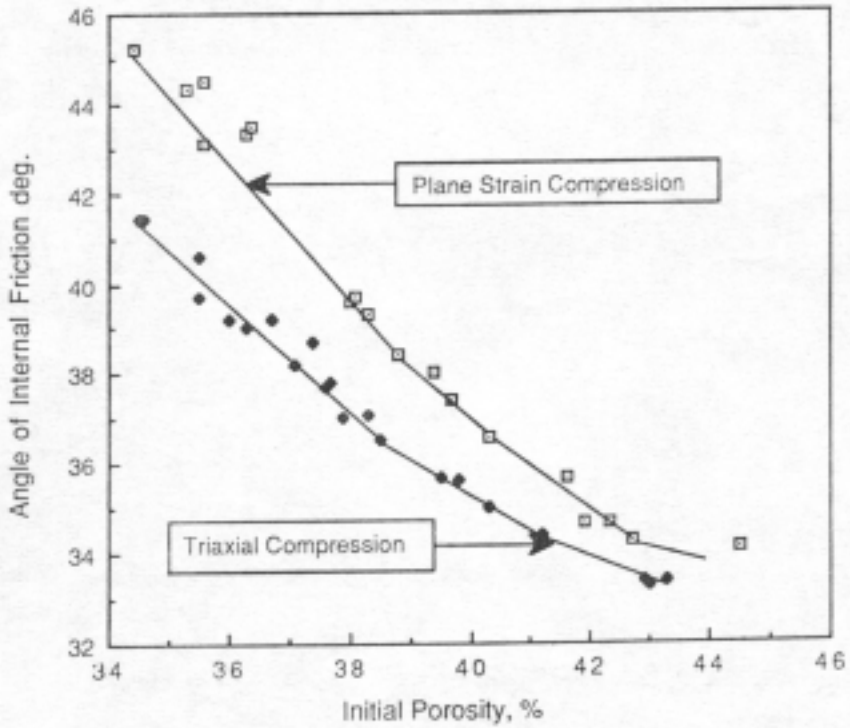

Fig. 36 Comparison of Angles of Internal Friction in Plane Strain and Triaxial Compression for Brasted Sand (Cornforth, 1964)

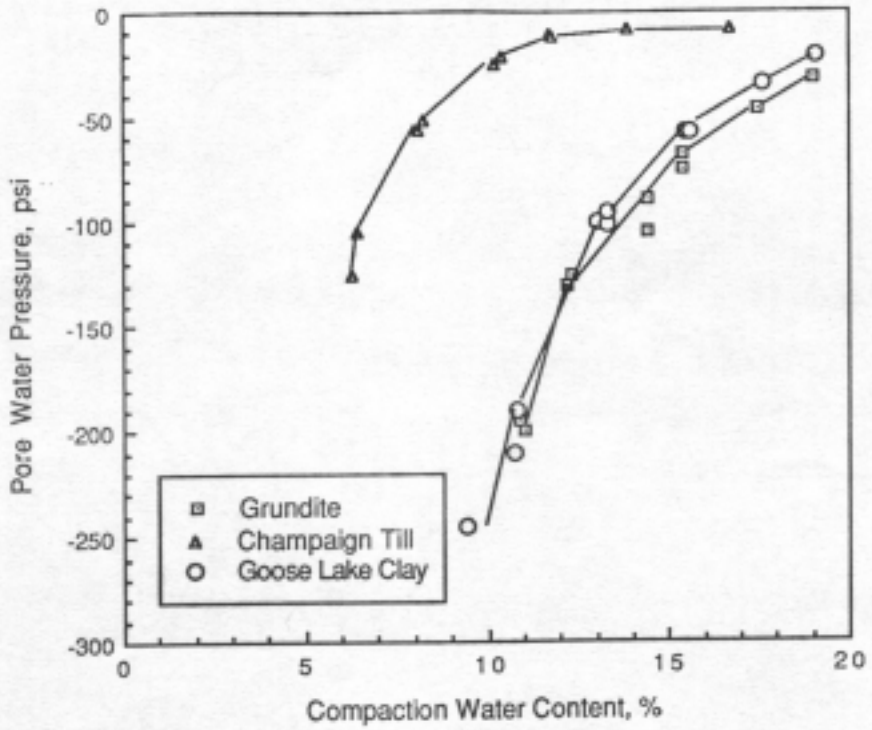

Fig. 37 Pore Water Pressures in Several Compacted Clays

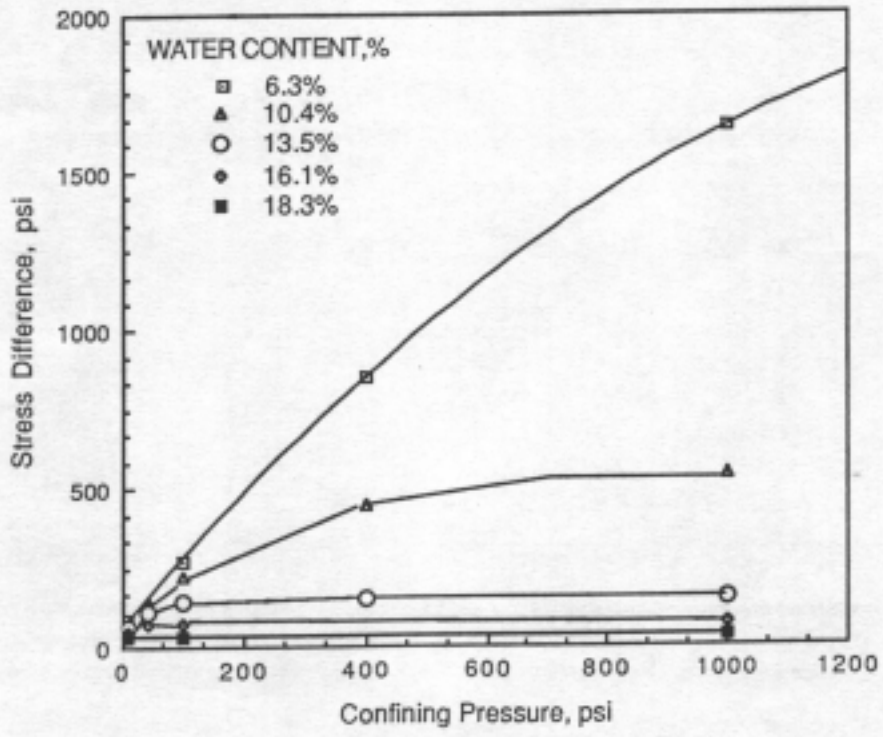

Fig. 38 Q-Type Failure Envelopes for Compacted Clay

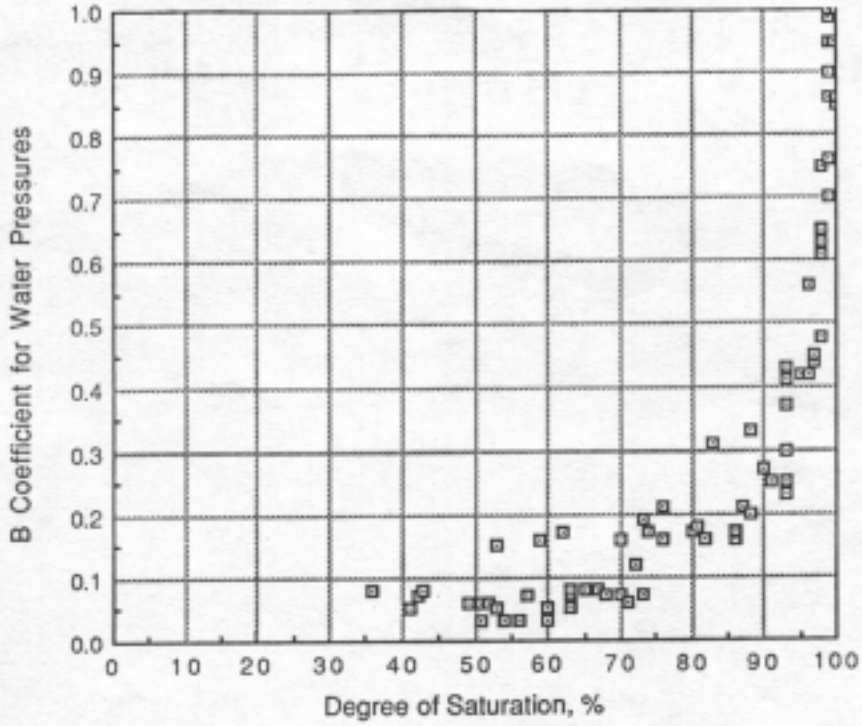

Fig. 39 Values of B Coefficient for Water Pressures for Compacted Champaign Till

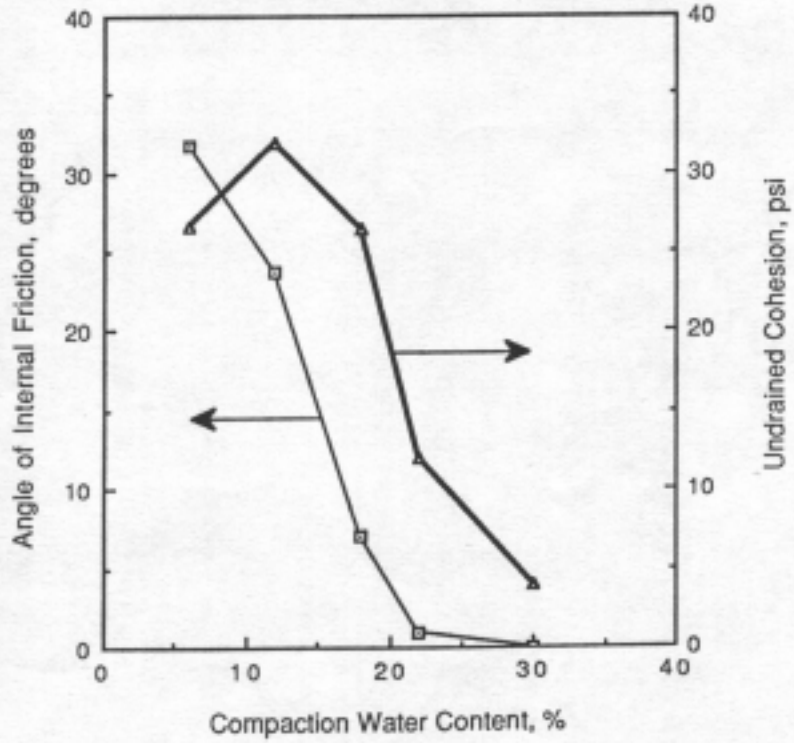

Fig. 40 Values of Friction Angle and Cohesion for Q-Type Triaxial Compression Tests on Compacted Taylor Clay